PERFORMANCE EVALUATION OF

SCALAR VERSUS VECTOR CONTROLLED INDUCTION MOTOR

FOR ELECTRIC VEHICLE APPLICATIONS

A Thesis

by

OWEN NICHOLAS GOLDEN

Submitted to the Office of Graduate and Professional Studies of
Texas A&M University
in partial fulfillment of the requirements for the degree of

MASTER OF SCIENCE

Chair of Committee,	Mehrdad Ehsani
Committee Members,	Karen Butler-Purry
	Shankar P. Bhattacharyya
	Reza Langari
Head of Department,	Jose E Silva-Martinez

August 2018

Major Subject: Electrical Engineering

ABSTRACT

In an effort to reduce dependence on fossil fuels, the automobile industry is adopting alternative fuel technologies for vehicles. One major contender for replacing the conventional internal combustion engine (ICE) vehicle is the electric vehicle (EV). The resurgence of EVs has been spurred by technology advances in motor design, power electronics and energy storage. Even with the advancement in technology, the emerging field still has much room for improvement. In order to make the EV practical, many challenges need to be met, at a minimum to the level of convention set by ICE vehicles, especially cost. The high cost of the EV is usually associated with the battery, nonetheless, the type of motor and controller can impact the price tag of the vehicle.

The type of motor best suited for EVs is the subject of many industry and academic research projects. In this study, a leading contender, the induction motor (IM), is explored because of its cost-effective characteristics. However, in order to achieve high performance, asynchronous motors, such as the non-linear IM, have complex electrical models and control methods when compared to their synchronous counterparts. This drawback affects the robustness and cost of the controller and, therefore, the vehicle. The literature in this area claims high performance control methods are necessary because of the dynamic nature of EV applications.

In this research, a comparative analysis will be given for two alternate control methods for the IM. Scalar controls are simple, robust, low-cost control methods based on the steady-state model of the IM. Despite its popularity in many industry

applications, several limitations confine scalar control to low performance applications. The majority of studies on IM control for electric vehicles focus on complex control algorithms, such as, field oriented control, a popular vector control technique. These studies often focus on small performance differences without any context. Due to its large inertia, the electric vehicle purposes a unique challenge that may be well suited for scalar control. The goal of this research is to compare the performance of an electric vehicle when utilizing these two different control methods and determine if the computationally intense vector control is required. The novelty of this study will be the emphasis placed on the modeling of the load (vehicle) and analyzing the results in terms of *meaningful* performance differences between the vehicles operating with the different control methods.

DEDICATION

To Simon.

ACKNOWLEDGEMENTS

I would like to take this opportunity to thank my committee chair, Dr. Mehrdad Ehsani for his guidance and support during this thesis. He is a great mentor, an excellent teacher and the ideal guide for research. His insight extends beyond the classroom. He has been a source of advice and encouragement while pursing my passion of becoming a professional electrical engineer. I would like to show my appreciation to Dr. Karen Butler-Purry, Dr. Shankar Bhattacharyya and Dr. Reza Langari for serving on my committee.

Thanks to my friends, colleagues and the department faculty and staff for making my time at Texas A&M University a great experience. Finally, thanks to my mother, father, sister, extended family and friends for their encouragement.

CONTRIBUTORS AND FUNDING SOURCES

Contributors

This work was supported by a thesis committee consisting of Professors Mehrdad Ehsani, Karen Butler-Purry, and Shankar P. Bhattacharyya of the Department of Electrical and Computer Engineering and Professor Reza Langari of the Department of Mehcanical Engineering.

All work conducted for this thesis was completed by the student, under the advisement of Dr. Mehradad Ehsani of the Department of Electrical and Computer Engineering.

Funding Sources

This thesis was supported by the Thomas W. Powell ’62 and Powell Industries Inc. fellowship from the Department of Electrical and Computer Engineering.

NOMENCLATURE

HEV	Hybrid Electric Vehicle
EV	Electric Vehicles
IM	Induction Motor
VFD	Variable Frequency Drives
EPA	Environmental Protection Agency
ICE	Internal Combustion Engine
ZEV	Zero Emission Vehicle
PM	Permanent Magnet
VVVF	Variable Voltage and Variable Frequency
IFOC	Indirect Field Oriented Control
DTC	Direct Torque Control
LMA	Loss-Minimization Algorithm
SSC	Simple State Control
SC	Search Control
LMC	Loss Model Control
DQZ	Direct-Quadrature-Zero
VSI	Voltage Source Inverter
CC-VSI	Current Controlled Voltage Source Inverter
FOC	Field Oriented Control
VIMM	Vehicle Inertia Measuring Machines

TABLE OF CONTENTS

Page

Page

LIST OF FIGURES

Page

Page

LIST OF TABLES

Page

1. INTRODUCTION

The world's energy infrastructure is largely dependent on fossil fuels. There are two problems with being reliant on this type of energy source. First, there is a finite amount of petroleum reserves. The development of highly populated countries, like India and China, are causing an increase in energy consumption and, therefore, an increase in the world's demand for fossil fuels. This leads to high fuel costs and dependency on foreign countries with the largest petroleum reserves. Second, there are growing concerns of the greenhouse effect caused by, in part, the CO_2 emissions associated with the burning of fossil fuel. In order to effectively fight climate change, a reduction of fossil fuel consumption must happen worldwide. This means alternative energy solutions must be viable for the majority of the world or, at least, for the major contributors to CO_2 emissions. These ecological and political pressures have caused substantial efforts worldwide to shift to alternative energy sources. With the transition away from fossil fuels, the transportation sector will have to adapt. The transformation is already underway in the automobile industry with the growing number of Hybrid Electric Vehicles (HEVs) and Electric Vehicles (EVs) in transit. Although the fleet of these alternative vehicles is small, the growth in popularity has sparked research in many electrical components, such as, batteries, power electronics, and electric motors.

HEVs are seen as a transitionary technology as they still require fossil fuel to operate. Alternatively, EVs do not require any fossil fuels and can be a long-term solution to meeting transportation needs in lieu of petroleum. However, the major

challenges facing EVs today are battery technology, recharging infrastructure, extended mileage range, and cost [1]. When overcoming these challenges, each component of the system needs to be considered individually and from a system level. The type, design, and control of the motor are important factors when addressing these challenges for the new application of EVs.

There are many types of electric motors that are being used for traction applications and the research continues on which provide the best total performance. The type of motor best suited for the vehicle depends heavily on the powertrain architecture and performance requirements. For EVs, the Squirrel-Cage Induction Motor (IM) is one leading contender. The IM's strengths are its cheap and robust design. The IM has an electrically isolated rotor that allows for high-speed operation and increased longevity, both attractive qualities for a traction motor. However, the IM is an asynchronous machine, which makes control more difficult than its synchronous motor counterparts. The control techniques for IMs have been the topic of numerous research papers. The type of control method is an important factor in the performance, reliability, and cost of the overall drivetrain.

There are several popular control methods for the IM. In this paper, the focus will be the on two fundamental branches used to control Variable Frequency Drives (VFD). Scalar controls are simple, well-known control method that uses the steady-state model of the motor to achieve desired operation. Despite its popularity in many industry applications, several limitations confine scalar controls to low performance or non-dynamic applications. In order to overcome the shortcomings of scalar controls, Field

Oriented Control (FOC) was conceived. The FOC concept was introduced by Hasse in 1969 and Blaschke in 1972. Using complex transformations to model the dynamic states of the IM, the control method marked an important paradigm in control of induction motors. Since the introduction, a number of control methods have been introduced that utilize similar models creating the family of vector control. This has led to a decline of research in scalar control methods especially for dynamic applications. EVs present a unique load for motor application. Although vehicles are considered a dynamic application, typically requiring vector controls, the large inertia of the vehicle mimics a 'semi-stiff' load. The time constants associated with electrical devices such as motors are significantly less than the time constants of a vehicle. These properties of vehicles may enable simplification of the motor control that has previously been thought to require complex, high performance control techniques, such as vector controls.

The goal of this research is to compare the performance of an EV using the two different control methods. The ingenuity of this research is analyzing the performance of the system with a realistic model of the vehicle. The results will also be evaluated from the vehicle's/driver's perspective, instead of drawing conclusion from generic models and loads, like much of the literature on this topic. The research requires designing the motor for EV application and accurately simulating the vehicle dynamics for a realistic drive cycle. The standardized FTP-75 urban drive cycle will be used to simulate an accurate, dynamic speed profile for the vehicle.

1.1. Motivation

The Paris Climate Accord is an agreement within the United Nations Framework Convention on Climate Change (UNFCC) between nearly all counties worldwide in order to reduce greenhouse gas emission. The agreement illustrates the world's determination to mitigate climate change effects by reducing the consumption of fossil fuels. According to the US Department of Energy, passenger transportation in the United States accounts for approximately 20% of the nationwide energy consumption which is almost entirely produced with fossil fuels [2]. Assuming consumption is similar in other industrialized counties, a solution for meeting the world's transportation needs in lieu of fossil fuels is of great importance.

Since climate change is a global problem, it must be addressed worldwide. The most significant factors in a worldwide solution are the most populated countries that are undergoing development and energy demand growth. The human population is growing rapidly. It is estimated that by 2050, the growth will start to slow down with a total population of 9.7 billion. At that point, India and China will be the most populated countries in the world at 1.7 and 1.3 billion, respectively. In comparison, the U.S. will have a population of approximately 400 million, only accounting for ~4% of the world population [3]. China has recently undergone a development period, which has led to a large increase in consumption of fossil fuels. India is currently undergoing a similar development with a growth in the middle class, leading to an increase in energy demands. Developing countries usually take the path of least resistance when it comes to meeting their growing energy demands. This means cheap and usually dirty/high

pollutant energy solutions. This is no exception for China and India. When addressing future transportation needs without fossil fuels, these countries need to be specifically considered. Alternative fuel transportation solutions must be tailored with these countries in mind. The transportation demands can be quite different in countries like China and India, as compared to the U.S. or other western countries. This is exemplified by the rickshaw in India. These small, low-cost, three-wheeled vehicles are extremely popular; it accounts for nearly $1/5^{th}$ of all urban transport. The Indian government recently had to outlaw a popular two-stroke rickshaw due to its pollution. Since the outlaw, cleaner rickshaws have penetrated the Indian transportation market. However, these improved rickshaws still depend on fossil fuels. The popularity of the rickshaw contrasts the stark difference between transportation needs in the U.S. and India. Notable differences are the size, cost, top speed, and range of these vehicles. Simply put, the solution must not be over engineered. This leads to an increase in price and a reduction in robustness which lowers its accessibility. Since India and China will play a larger role in the consumption of fossil fuels in the future, it is important to understand these foreign markets and how best to impact their transportation fleet [4].

There are several technologies being developed to replace conventional fossil fuel dependent Internal Combustion Engine (ICE) vehicles. Some of these include biomass, fuel cells, hybrid electric powertrains, and pure electric vehicles. All these technologies have certain advantages and disadvantages associated with them. In this space, there are several competing technologies, but HEVs & EVs are promising. These technologies have the most penetration in the current fleet than any other alternative fuel vehicles. In

order to achieve zero emission vehicle (ZEV) or semi-ZEV status, either a series HEV or EV topology must be utilized [1]. The machinery of these two vehicles are quite similar because they both drive the wheels with electric powertrains. However, these vehicles still struggle with high cost. The high cost of EVs is closely associated with the cost of the batteries, but also include the motor, power electronics, and controls. In order to reach growing markets that carry significant weight for combating climate change, such as India, it is necessary to drive down the cost of these vehicles and improve robustness. One way to effectively lower the cost of these vehicles is the choice of the traction motor.

1.2. Traction Motors

The debate for which motor is best suited for EVs continues to be discussed among researchers and industry leaders. There are a variety of options when it comes to choosing an electric motor and each type comes with its own set of advantages and disadvantages. The decision of the type of motor depends heavily on its application. As shown in the figure below, motors are broken into two categories.

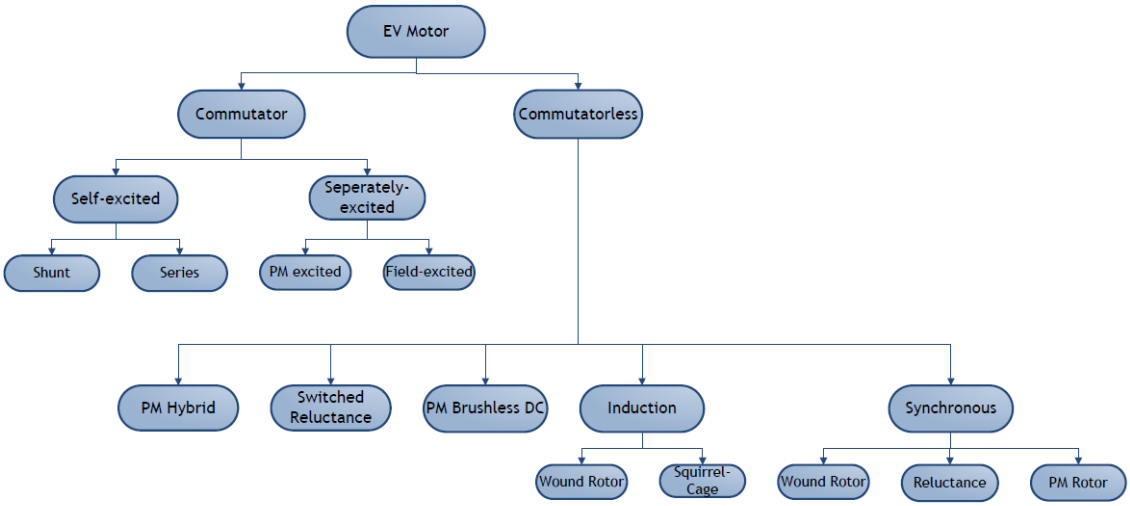

Figure 1 : Traction Motors

Motors that require commutators are uncommon in EV applications due to the regular maintenance that is required to replace commutators. Under the commutatorless (or brushless) branch, the squirrel-cage induction motor and permanent magnet (PM) motor are two of the most popular for EVs. The PM motors have some strong advantages over the induction motor, such as, high power density and higher efficiency at certain operating conditions. However, the efficiency of a PM for the entirety of the drive cycle is similar to an IM due to the wide range of operating conditions. This is achieved by the IMs ability to field weaken. Additionally, PM motors require rare-earth magnets that increase the cost. The limited availability of these magnets can drive up the cost. This reliance on rare, expensive materials does not make PM motors an ideal candidate for a high volume, inexpensive EV. On the other hand, IMs are lightweight, efficient, low cost motors. This makes it an ideal candidate. One of the challenges associated with induction motors is its control. Since the rotor and electrical frequency

do not have the same rotational speed, the motor is defined as an asynchronous machine. This, paired with the non-linear characteristics of the IM, make control difficult compared to its synchronous counterparts.

1.3. Control Methodology for Induction Motors

Induction Motors are operated using AC signals. In order to control these machines for a wide speed range, the power electronics need to supply a variable voltage and variable frequency (VVVF). There are several minimum requirements a control method for a traction motor must meet to be satisfactory. It must be able to provide any torque below, or equal to, rated torque for any operating speed below rated speed. Additionally, the motor must be able to operate in field weakening region, this is especially important for EV applications because vehicles require wide speed ranges. Finally, for dynamic systems, the control method needs to meet the changing torque demands in adequate time so that the performance of the system satisfactory. There are a variety of control methods for the IM. The type of control has a large impact on the performance, cost, and robustness of the system. As shown in Figure 2, these controls fall under two categories: scalar and vector controllers.

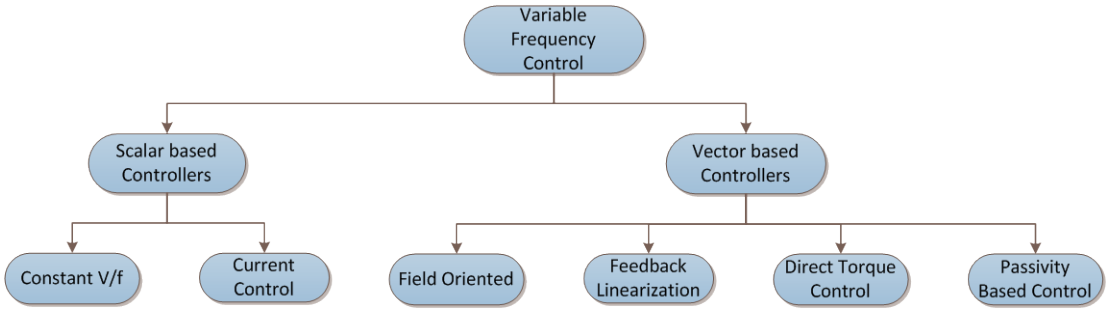

Figure 2 : Control Methodology for Variable Frequency Control

Scalar controllers are based off the steady-state model of the IM. These controllers are common in industry, but are often limited to pumps, fans, conveyor belts. These applications do not demand quick dynamic torque changings during operation. The common limitations associated with scalar are low speed performance, dynamic torque response, and coupled torque and field flux quantities. These shortcomings were overcome with the introduction of Field Oriented Control by Hasse in 1969 and Blaschke in 1972. This was the origin of vector controls based on the dynamic model of the IM. Vector controls are more complex and expensive than scalar, often requiring accurate parameter knowledge or rotor flux position [5] [6]. However, vector controls are able to achieve great performance. It has fast dynamic torque response, good low speed performance, and decoupled torque/flux quantities.

As will be shown in the literature review, scalar is often disregarded as an appropriate control method for EV applications because of its poor dynamic response. The core of this research questions the effect of this slow dynamic response on a passenger vehicle. In section 1.4, the effects of these different torque responses will be explored briefly. This will illustrate the inspiration for this study.

1.4. Torque Response & Vehicle Dynamics

As seen from the driver, the traction motor is a torque generator. The driver demands the desired torque to accelerate the vehicle to its intended speed. Like a PI controller, the driver searches for the appropriate torque. This leads to steadily changing acceleration profiles. Even for the most stringent circumstances, this acceleration ramp last for 100's of milliseconds as the driver's foot searches for a suitable torque. This

gradual acceleration or torque demand is specific to vehicle applications. However, it is not considered in the past traction motor research. Instead, it is common practice for motor controls to be designed for tracking a speed ramp which corresponds to an instantaneous torque demand or step torque. But, this does not model the practicalities of a driver or vehicle applications. This "overkill" method commonly used in traction design will be discussed in the literature review in the following chapter. The following example will take into consideration the worst-case scenario in terms of torque demand and demonstrate the response of a highly inertial load (like a vehicle) for a step versus ramp torque. This will illustrate that even the "overkill" approach does not demand a stringent torque response requirement.

The following simplified equation can describe the behavior of the load.

$$T_e = J_{total} * ({}^{d\omega_{rotor}}/_{dt}) \tag{1.1}$$

where

T_e = electromagnetic torque;

J_{total} = total inertia of system;

ω_{rotor} = rotational speed of rotor;

d/dt = time derivative;

In general, (1.1) has terms for viscous friction and load torques that have been omitted for simplicity. The response time of the electromagnetic torque is determined by the type of control method. As mentioned previously, the response time can be an order of magnitude larger for scalar motor controls. Nonetheless, the speed response of the vehicle is dictated by the driver and the large inertia for the vehicle, J_{total}. This inertial term consists of components from the motor and vehicle; the specifics of this term are

discussed in section 4. A simple demonstration can show the effects of a delayed developed torque on this 'semi-stiff', high inertial system.

The worst-case scenario can be imitated by demanding the rated torque from standstill. As shown in (1.1), the torque and inertia are required to determine the speed response of the vehicle. The exact values for the rated torque and inertia of an electric vehicle, and how they are attained, will be discussed in sections 4 and 5. For this example, approximate values will be assigned for these variables. The values chosen exemplify a motor and chassis for a common commuter vehicle. In section 5, the steps to determine the exact size of the motor and other design parameters are given in detail. For this demonstration the values are as follows: the rated torque is ~180 Nm, gear ratio is 10:1, and total inertia is ~100 kg*m^2. The gear ratio is required to determine the speed of the vehicle and the total inertia of the system. Again, these values will be justified in section 4.

In order to demonstration the different performance between torque responses, an ideal controller that delivers torque instantaneous will be compared to a slowly ramped developed torque that takes 200ms to reach demanded torque. This simulation will mimic vector (fast dynamic response) and scalar (slow dynamic response) controls. Now the simulation can be run to compare an instantaneous versus delayed torque (step versus ramp).

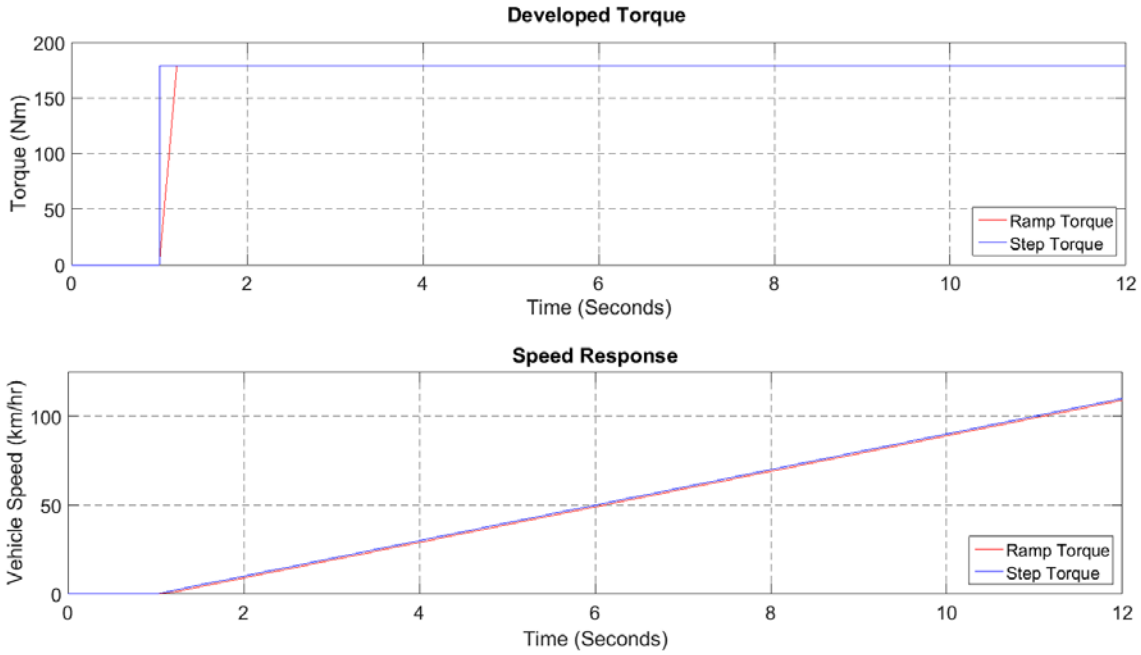

Figure 3 : Torque and Vehicle Speed with Stepped versus Ramped Torque

At one second, a torque is applied to the load. The load is modeled as a vehicle of 1500 kg with the specifications mentioned above, and the dynamics are described by (1.1). Two simulations were done. One with a step torque of 180 Nm where the torque is instantaneously produce (Blue). Another with a ramp torque (Red). The ramp torque takes 200 ms to reach 180 Nm. This leads to a short period of 200 ms time where the vehicle acceleration is below the desired value. After this short period, there is a speed discrepancy of 1 km/hr between the two simulated vehicles. The vehicle supplied with a ramped torque reaches 100 km/hr at a time of 11.10 sec, while the step torque achieves this in 11 sec. The effect of this slower developed torque is a small speed discrepancy and a delay in acceleration to desired speed of 100 ms. In conventional motor control research, this delayed torque would be seen as a substantial performance difference

(exaggerated by simulated low inertial loads). But, the large inertia of the vehicle causes the speed divergence to be small and insignificant for vehicle applications and would go unnoticed by any driver. Furthermore, for commuter cars, a sharp demanded torque is not realistic; usually a gradual application of torque is demanded by the steady pressing of the pedal. The driver, upon perceiving any speed discrepancy or acceleration delay, would simply press harder on the accelerator pedal to compensate. This scenario demonstrates an extreme case because no motor control can deliver an instantaneous step torque, nor would the driver demand such a torque. Moreover, the system modeled here assumes to be 100% stiff with no dampening. In reality, the motor shaft, gears and tires would all dampen the torque step, which would reduce the discrepancy between the two systems.

In light of these results, the proposition of this research is that the slower developed torque of scalar controls will not affect the overall performance of the vehicle in any meaningful way. This theory will be tested in our simulations.

1.5. Research Objectives

Based on the information laid out in this section and the literature survey provided in the next section, the following are the objectives for this thesis work:

- An accurate model of a high inertia, vehicle load will be created. Using the FTP-75 urban drive cycle, a realistic speed profile for a dynamic drive cycle will be provided. Reasonable vehicle performance parameters will be chosen to exhibit a common passenger vehicle.

- A dynamic model of the induction model will be created using Simulink. The rated power size, torque and speed for the motor will be designed specifically for an EV based off the performance requirements of the vehicle. Then, accurate parameter values for this sized motor will be established.
- Finally, the control methods will be tested in several ways. First, during the start of the vehicle. Second, by tracking the FTP speed profile. Once the controls have been simulated, the performances will be compared. The low speed performance, dynamic torque response for these methods will be studied.

1.6. Outline of this Thesis

The following sections cover the topics of motor control, vehicle dynamics, simulation techniques, results and conclusions.

Section 2 is an overview of the scene of the literature pertaining to IM motor control performance, both for generic and EV applications. The section reviews the standard process of evaluating motor control performance and the subsequent conclusions from these evaluations. The discussion includes reasons as to why these conclusions may not be accurate in the case of EVs. Additional areas of interest are identified and particular attention will be paid to these areas throughout the paper.

Section 3 gives a description of the IM. This section discusses the general physics behind the induction motor, the steady-state and dynamic electrical models, and operating techniques.

Section 4 and 5 cover the vehicle dynamics and the design of the electric motor. These sections give a background in the forces and power demands of a vehicle. These details are often left out of motor control research and will play an important role determining the performance impacts of the various controls from a vehicle/driver's perspective.

In section 6, the model of the induction motor, control loops, and vehicle dynamics are given. The block diagrams in Simulink are presented and the details of the logic are given with the information outlined in sections 2-5 in mind. Assumptions and omissions are acknowledged. The impacts of these assumptions are discussed.

Finally, in section 7 and 8, the results and conclusion of the research are given.

2. LITERATURE REVIEW

The performance difference between scalar and vector control methods has been the topic of numerous research. Many of these studies focus on general motor applications. These investigations tend to use generic motor designs, speed profiles, step load torques, and low inertia loads. In these conditions, the performance differences between the controls are pronounced; this leads to a common conclusion that scalar is unfit for dynamic applications. However, the simulation environment is not an accurate representation of a vehicle and, furthermore, the performance differences are not indicative of the driver's experience. Nevertheless, studies pertaining specifically to EV applications dismiss scalar altogether as a viable option due to the aforementioned literature.

The following sub-sections will analyze the research in the areas related to general induction motor controls and controls for traction applications. The concerns and conclusions from these papers will be addressed in the conclusion of this study.

2.1. Standard Motor Control Studies

The majority of motor control studies do not consider specific applications of the motor. Instead, many of these studies use generic speed ramps and step load torques in order to test the performance of the controls. These constraints lead to valid observations of degraded performance; however, some of the exposed shortcomings are not significant when driving a unique load, such as a vehicle.

In the analysis done by Sharma and Garg in [6], they compare scalar and vector controls of an induction motor. The study uses a small 3 HP IM. The test is done using only the inertia of the rotor, which is quite small, and applies step load torques of 5, 10, and 12 Nm. The motor is to track a speed ramp to 500 RPM in 250 ms. The entire simulation last 3 seconds. Three control loops are tested: open-loop constant V/f (a type of scalar), closed-loop constant V/f, and indirect field oriented control (IFOC). The results show IFOC's ability to track the reference speed nearly perfectly with little error, while the closed-loop constant V/f has poor starting performance with overshoot due to the tuning of the PI controller. The study concludes, scalar or V/f has "poor transient response, unsatisfactory speed accuracy at low speed regions, sluggish response and inability to control two important variables i.e. torque and magnetic flux" continuing that it should "not [be] used in high performance applications". However, if the results are put in context of electric vehicle applications, the poor transient and sluggish response play an insignificant role for vehicle applications as was shown in section 1.4. Additionally, for driving applications, the speed regulation is accomplished by the driver. The type of quick response and overcompensation behavior emulated by the PI controller does not simulate a driver. Drivers do no demand steep step torques as it is uncomfortable for the passenger to accelerate the vehicle so suddenly. Furthermore, humans cannot perceive many of the effects highlighted in this simulation because of the small timescales. The heavy body of the vehicle would filter out many of the variations in speed of a poorly controlled motor. On the other hand, the study does demonstrate poor speed accuracy at low speeds and the inherent coupling of torque and magnetic

flux. These issues are concerns for use in EVs, but the impact is still unknown and will be explored in this paper. The study continues with its conclusion of vector control or IFOC. It concludes that the vector control does not exhibit any of the transient or response issues associated with scalar. This makes it a good candidate for high performance applications. However, the control "is a complex and high price control technique". Over the course of this paper, the necessity of this type of high performance for vehicles will be examined.

Similar studies are presented in [7] and [8]. These papers use different sized motors, but the procedure and conclusions are identical to [6].

2.2. Survey of Control Schemes for Electric Vehicles

In addition to the aforementioned studies, there has been research conducted specifically related to EV applications. Yet, these contributions either overlook scalar controls completely or fail to design/size the motor and model the loads associated with vehicle applications.

[9], [5], and [10] are several of the works that examine the performance of vector control methods for EVs such as Direct Torque Control (DTC), direct and indirect FOC. These papers focus on vector controls because "most […] control strategies are only able to overcome speed performance, but are weak in the dynamic response. Therefore, more complex control strategies must be used" [10]. Scalar is not seen as a feasible option for EVs to warrant examination. As was shown in the introduction, the effects of slow dynamic response may be overstated.

Conversely, the work by Ellabban, Mierlo, and Lateire in [11] explores scalar, as well as, two vector control methods for vehicle applications: Indirect FOC and DTC. This research follows the same performance tests that were mentioned in the previous section. There is no discussion of vehicle dynamics, which undermines the importance of the application when analyzing the performance of the control. Additionally, the motor was not designed for EV application. For example, it is common practice to use a high-speed motor and gear it down to the speed of the wheels. This reduces I^2R losses and minimizes the physical size of the motor. This is an important design consideration when building an EV. However, this is not considered in this research. Instead, the motor only has a rated speed of 1500 RPM. The study does not use accurate speed profiles with realistic load torques for a vehicle; instead, it uses generic profiles to test the performance. Furthermore, the conclusion does not include any thought of how these differences would be perceived by the driver.

This is an important distinction between the past research and the research presented in this paper. The research should not be which control method has the best overall performance, but which method is appropriate for EV applications.

2.3. Efficiency Optimization

After the review of the literature, a couple of common concerns for scalar controls were identified: dynamic response and low speed performance. The impact of these features will be the primary focus of this research. Efficiency is not a common distinction between scalar and vector controls in the literature mentioned above, but it is cited in other studies. In [12], it is stated that the overall efficiency of the motor can be

improved by vector. The efficiency optimization of an induction motor is a popular field of study and will be reviewed to understand how this is possible.

In general, an induction motor is designed to run at rated condition. The design of the motor considers many factors in order to minimize the losses of the machine. There are five categories of losses: stator copper, rotor copper, iron, mechanical, and stray [13]. The design of the motor considers all of these losses in order to minimize them during rated condition. A study of the copper and core losses reveals that the optimization of one oppose the other. In other words, decreasing copper losses, increases iron losses and vice versa. A point that minimizes both losses can be found to optimize the motor efficiency [13]. However, the design of the motor only allows for optimization at rated conditions. But, during the vehicle's drive cycle, the motor operates in a variety of conditions.

At light loads and low frequency operation, the losses in the copper and iron are not optimized as is at rated conditions. If using a common scalar control called constant V/f, the field flux is held at a constant, rated value throughout operation. This leads to over-excitation of the rotor because rated flux is not required for light loads. The over-excitation causes both the losses in copper and iron to increase relative to the delivered power. In [14], they examine a loss-minimization algorithm (LMA) that utilized vector controls ability to control field flux and torque independently. The study provides an insightful efficiency curve of the two control methods.

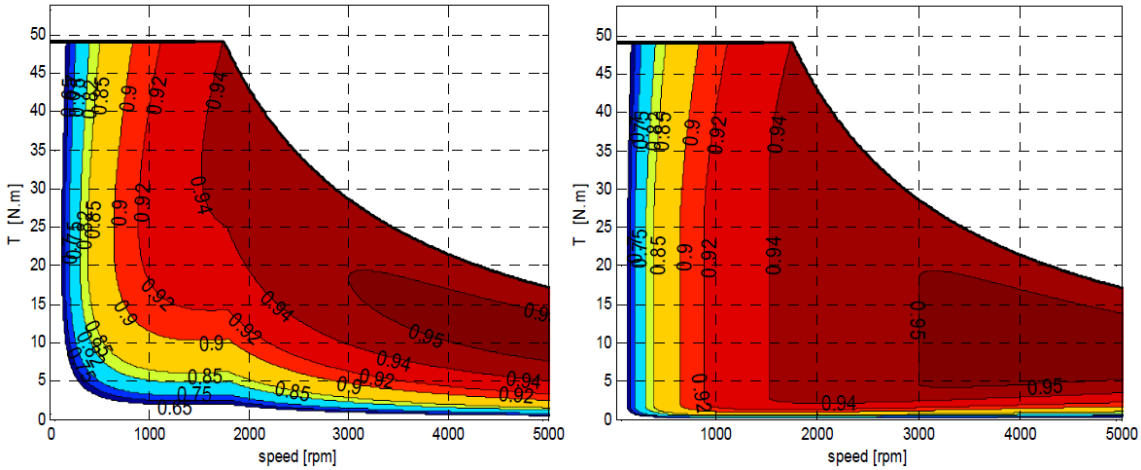

Figure 4 : Efficiency Curve (Constant Field & Loss-Minimization Algorithm)[1]

On the left, the efficiency curve shows an induction motor controlled with the simple constant V/f, scalar method. While the right shows a vector control with a loss-minimization algorithm. The areas of importance are the operating points at low speed & low torque. This illustrates the effects of over-excitation during constant field operation. Vector controls, on the other hand, is capable of weakening the flux during these operations, and therefore, minimizes the losses. However, these efficiency optimizations may not require the complex controls associated with vector controls. There have been numerous studies done on difference techniques to optimize operation of induction motors. A review of three of the common methods, Simple State Control, Loss Model Control and Search Control, will be given to determine if vector controls are necessary for efficiency optimization.

[1] *Reprinted with permission from "Evaluation of an Energy Loss-Minimization Algorithm for EVs Base on Induction Motor" by Melo P, De Castro R, Esteves Araujo R., 2012. *Induction Motors – Modelling and Contro*l, Ch. 17, Copyright 2012 by CC BY 2.0 License. Available from: http://dx.doi.org/10.5772/52280

Simple State Control (SSC) either measures or estimates the value of a certain variable, then uses a feedback loop to control the value to a predefined reference value which minimizes losses. The common variables used for this strategy is slip frequency or power factor displacement. Slip frequency requires speed and load knowledge of the motor. This method estimates values based off motor parameters and, therefore, is sensitive to parameter changes due to temperature and magnetic saturation. Furthermore, load knowledge is difficult to predict with a vehicle. Power factor displacement, on the other hand, does not require speed or load information. The displacement is measured from power measurements that are usually required for battery safety purposes. However, determining optimal power factor can be tedious, typically requiring trial and error [13]. The method does not rely on whether the steady-state or dynamic IM model is used for the control method and, therefore, could be implemented with scalar or vector control.

Loss Model Control (LMC) computes the losses in the machine and selects the flux that minimizes the losses. This algorithm can utilize either scalar or vector motor models. The convergence time of the algorithm depends on the implementation, application and motor. The settling time varies from 100's of milliseconds up to multiple seconds. For a vehicle application, these are small time scales when considered overall drive cycles. Nevertheless, the motor model relies on parameter values and estimation, which means the algorithm is parameter dependent. The technique is still a viable option for optimization because of its ability to use scalar motor models [13].

However, this will require significant tuning to the vehicle. The settling time can affect the performance of both controls.

Search Control (SC) methods utilize on-line procedures to determine optimal operating conditions. The stator and rotor flux are decremented until the measured power value settles on a minimum. Unlike the pervious methods, SC does not depend on parameter values. Still, there are several challenges when applying SC. The method can lower flux and cause the motor to be sensitive to load perturbations. Additionally, tuning the control is important in order to avoid oscillatory behavior about the minimal flux value. As mentioned for LMC, this method takes time to converge on a value, but vehicle applications are forgiving for these small-time scales.

In order to minimize the weaknesses of these techniques, there are hybridize methods that combine controls to attain good features of the optimization strategies. Artificial Intelligence techniques like artificial neural networks and fuzzy logic are also promising optimization tools for IM optimization [13].

An example of a few options for efficiency optimization techniques for scalar controls is given in [15]. The paper includes voltage perturbation, speed control, and a slip compensator as efficiency methods. The paper concludes that “improvements in motor/drive efficiency are achieved from 2% to 16% [15].

The field of efficiency optimization for induction machines is an extensive one. Deciding on a solution requires research and tuning to the application. This is especially tedious for vehicle application because field weakening will decrease the torque response time of the IM. Therefore, there is a tradeoff in performance and efficiency

that must be studied to ensure the vehicle is operable at these low torques and speeds. The technique chosen will also put performance requirements on the controller. Since it has been shown that the optimization technique does not require vector, the focus of this research will continue to investigate scalar's application for vehicles without further examination into efficiency optimization.

3. SQUIRREL-CAGE INDUCTION MOTOR

There are two basic types of induction motors: wound-rotor and squirrel-cage. Wound-rotors tend to be less popular because of their high cost, required maintenance, and less rugged design [16]. These characteristics are especially undesirable for EV applications. The use of squirrel-cage IMs is so common that it is often implied when not explicitly stated. For the remainder of this paper, any reference to an IM refers to this squirrel-cage design. The simplistic structure of a squirrel-cage IM is shown in the figure below.

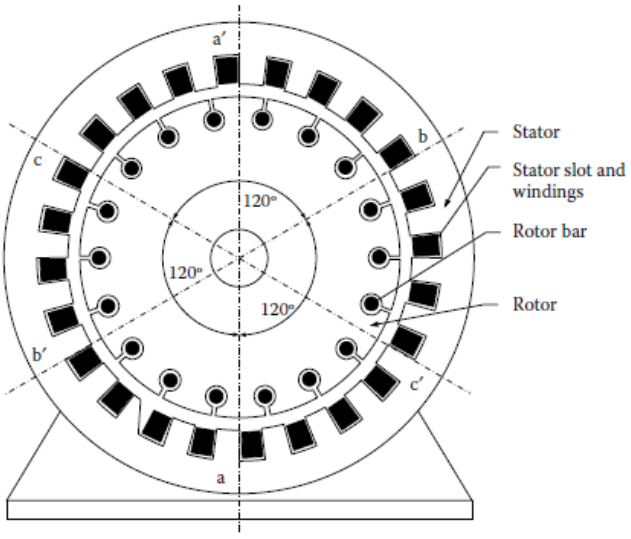

Figure 5: Cross Section of Squirrel-Cage Induction Motor [16][2]

[2] *Reprinted with permission from *Modern Electric, Hybrid Electric, and Fuel Cell Vehicles*, by M.Ehsani, Y. Gao, A. Emadi, 2010, CRC Press, Boca Raton, FL. Copyright 2010 by Taylor and Francis Group, LLC

The stator of an induction motor is no different from many of its AC motor counterparts; however, the rotor design is significantly different. As shown above, the rotor consists of rotor bars that are short-circuited together at both ends (not shown). This 'cage' cuts the rotating stator magnetic field. Faraday's law of induction described the resulting voltage (ε) generated by the changing flux linkage (λ) through the rotor bars.

$$\varepsilon = \frac{d\lambda}{dt} \tag{3.1}$$

The voltage generated in the rotor produces a current, which in turn, creates a magnetic field. This is the general principle of how the IM operates. From this overview, the major advantages of the motor can be deduced. The electronically isolated rotor allows for a simple, low-cost design that is robust in nature. However, the rotor flux is only produced when there is a changing flux through the rotor bars. Therefore, in order to produce a torque, the rotor cannot be rotating at the same speed as the stator flux. This introduces the concept of 'slip'. Slip is defined as the difference between the rotational speed of the stator flux and the mechanical speed of the rotor. There are several ways to discuss slip, as a normalized quantity, *s*, or as a speed/frequency, ω_{sl}.

$$s = \frac{\omega_s - \omega_m}{\omega_s} \tag{3.2}$$

$$\omega_{sl} = \omega_s - \omega_m = s * \omega_s \tag{3.3}$$

where

s = slip;

ω_{sl} = slip frequency;

ω_s = stator flux frequency;

ω_m = mechanical rotor frequency;

Slip plays an important role in the torque produced by an IM. In order to better understand slip, and the operation of an induction motor, it is helpful to study the steady-state operation.

3.1. Steady State Model of Induction Motor

The IM converts electrical energy into mechanical energy, or, vice versa. Any electrical device can be studied using an electrical circuit. The following diagram illustrates the per-phase steady state circuit analysis of an IM.

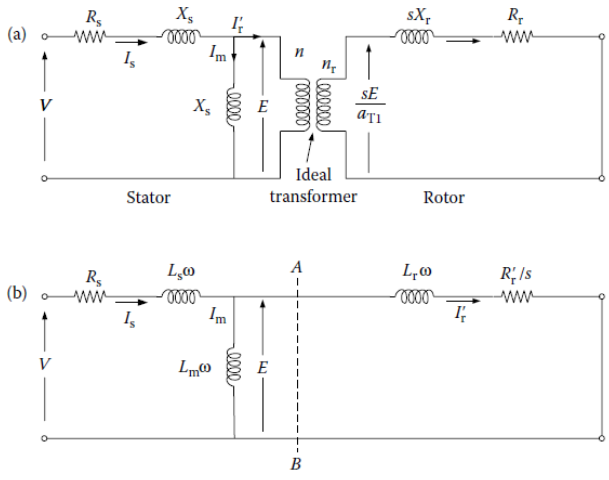

Figure 6 : Equivalent Circuit of IM a) with Transformer b) No Transformer [16][3]

[3] *Reprinted with permission from *Modern Electric, Hybrid Electric, and Fuel Cell Vehicles*, by M.Ehsani, Y. Gao, A. Emadi, 2010, CRC Press, Boca Raton, FL. Copyright 2010 by Taylor and Francis Group, LLC

The electronic isolation between the stator and rotor (or the airgap) is modeled after an ideal transformer in Fig. 6 a). However, the rotor quantities can be reflected to the stator frame. This is illustrated in Fig. 6 b). After the reflection, the circuit in Fig. 6 b) is illustrated as a single circuit even though it describes two separate circuits, the stator and rotor.

The graph below shows the torque-speed curve for an induction motor in steady state. The stable operating region for the IM is on the right-hand side of this curve. The three different frequencies are shown on the x-axis. It can be seen that the value of the slip speed, ω_{sl}, determines the developed torque. This relationship can be approximated as linear for highly efficiency induction motors. With knowledge of the rotor speed, the linear relationship between torque and slip can be utilized to find the electrical frequency, ω_s. This simple technique is one of the base principles of scalar that will be discussed later.

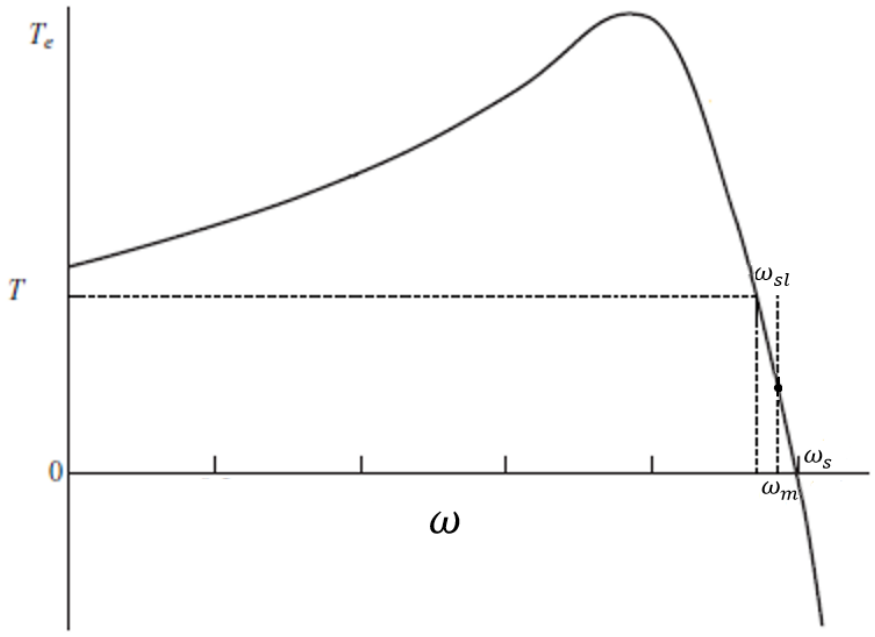

Figure 7 : Torque-Speed Curve for IM [17][4]

However, this torque-speed curve only represents the steady state mode. The performance can be quite different in dynamics situations. The torque on a free to accelerate load is shown in the curve below.

[4] *Reprinted with permission from *Analysis of Electric Machinery and Drive Systems*, by P. Krause, O. Wasynczuk, S. Sudhoff, S. Pekarek, 2013, IEEE Press, Piscataway, NJ. Copyright 2013 by IEEE, Inc.

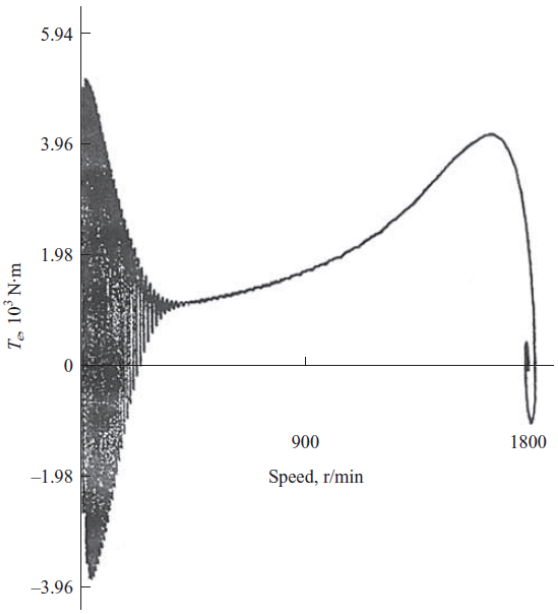

Figure 8 : Free-Acceleration Torque Curve [17][5]

The motor in this simulation has the rated voltage and frequency applied at stand still. The curve reveals that the steady state model does not accurately predict transient and dynamic behavior, especially at start-up. The torque oscillations at the start have an average positive torque that accelerates the rotor/load. The oscillations in torque are created by the interaction between the synchronously rotating magnetic field of the rotor and the stationary field produced by the DC component of stator current. This DC component is produced from the sudden application of voltage across the inductive windings of the stator.

This effect, along with others, is not addressed by the steady state model of the induction motor and, in turn, scalar control techniques. During this study, the

[5] *Reprinted with permission from *Analysis of Electric Machinery and Drive Systems*, by P. Krause, O. Wasynczuk, S. Sudhoff, S. Pekarek, 2013, IEEE Press, Piscataway, NJ. Copyright 2013 by IEEE, Inc.

shortcomings of applying a steady state control method to a dynamic application will be observed. It will be determined whether this causes significant degradation to the performance of the EV and, if so, can it be corrected without resorting to the complexities of vector controls.

It will be important to model the dynamic behavior of the induction motor, even when applying a scalar control, so that these effects, like the torque oscillation mentioned previously, can be observed.

3.2. Dynamic Mathematical Model for Induction Motor

The following equations describe the dynamics of the stator and rotor circuits. Notice the voltages for the rotor are zero for a squirrel-cage IM because the rotor bars are shorted.

Stator Equations:

$$v_{as} = r_s i_{as} + \frac{d}{dt}\lambda_{as} \tag{3.4}$$

$$v_{bs} = r_s i_{bs} + \frac{d}{dt}\lambda_{bs} \tag{3.5}$$

$$v_{cs} = r_s i_{cs} + \frac{d}{dt}\lambda_{cs} \tag{3.6}$$

Rotor Equations:

$$v_{ar} = 0 = r_r i_{ar} + \frac{d}{dt}\lambda_{ar} \tag{3.7}$$

$$v_{br} = 0 = r_r i_{br} + \frac{d}{dt}\lambda_{br} \tag{3.8}$$

$$v_{cr} = 0 = r_r i_{cr} + \frac{d}{dt}\lambda_{cr} \tag{3.9}$$

where

v_{as}, v_{bs}, v_{cs} = three-phase stator voltages;

i_{as}, i_{bs}, i_{cs} = three-phase stator currents;

λ_{as}, λ_{bs}, λ_{cs} = three-phase stator flux linkage;

r_s = stator resistance;

v_{ar}, v_{br}, v_{cr} = three-phase rotor voltages;

i_{ar}, i_{br}, i_{cr} = three-phase rotor currents;

λ_{ar}, λ_{br}, λ_{cr} = three-phase rotor flux linkage;

r_r = rotor resistance;

d/dt = time differentiation;

Solving the three-phase differential equations can be difficult due to the coupling between the stator and rotor inductances. Below is an example of one of the flux linkage equations for phase A.

$$\lambda_{as} = L_{as,as}i_{as} + L_{as,bs}i_{bs} + L_{as,cs}i_{cs} + L_{as,ar}i_{ar} + L_{as,br}i_{br} + L_{as,cr}i_{cr} \qquad (3.10)$$

where

$L_{as,xx}$ = mutual inductance between Phase-A stator and XX;

i_{as}, i_{bs}, i_{cs} = three-phase stator currents;

i_{ar}, i_{br}, i_{cr} = three-phase rotor currents;

The flux linkage of phase-A depends on the mutual inductances between the stator and rotor windings, terms: $L_{as,ar}$, $L_{as,br}$, $L_{as,cr}$. These terms depend on the position of the rotor (θr). This dependence makes solving the differential equations difficult. However, it can be made simpler by using reference transformations. Using a Clarke transformation, the three-phase IM circuit can be transformed into a virtual two-phase reference frame called the DQ-frame. One of the main advantages of this transformation

is the removal of the θr dependence because the phases are in quadrature and the symmetry of the 'virtual' two-phase machine.

3.3. Direct-Quadrature-Zero (DQZ) Model

The direct-quadrature-zero (DQZ) or sometimes simply called DQ transformation is accomplished by using a Clarke transform to convert the three-phase system to a two-phase. Then, a Park transform can be used to rotate the two-phase system about the z-axis. The transformation is shown for an arbitrary vector, $\boldsymbol{f}_{abc}$, with the Clarke and Park transforms combined in matrix $\boldsymbol{K_s}$. The speed at which the reference frame rotates is dictated by the change of θ. The usefulness of rotating the reference frame will become apparent when discussing vector control strategies.

$$\boldsymbol{f}_{qd0} = \boldsymbol{K}_s \boldsymbol{f}_{abc} \tag{3.11}$$

$$\boldsymbol{f}_{qd0} = \begin{bmatrix} f_q \\ f_d \\ f_0 \end{bmatrix} ; \boldsymbol{f}_{abc} = \begin{bmatrix} f_a \\ f_b \\ f_c \end{bmatrix} \tag{3.12}$$

$$\boldsymbol{K_s} = \frac{2}{3}\begin{bmatrix} cos\theta & cos\left(\theta - \frac{2\pi}{3}\right) & cos\left(\theta + \frac{2\pi}{3}\right) \\ sin\theta & sin\left(\theta - \frac{2\pi}{3}\right) & sin\left(\theta + \frac{2\pi}{3}\right) \\ \frac{1}{2} & \frac{1}{2} & \frac{1}{2} \end{bmatrix} \tag{3.13}$$

Once the transform has been applied to the three-phase IM, the following circuit diagrams model the new two-phase system for an arbitrary reference frame rotating with an angular velocity, ω.

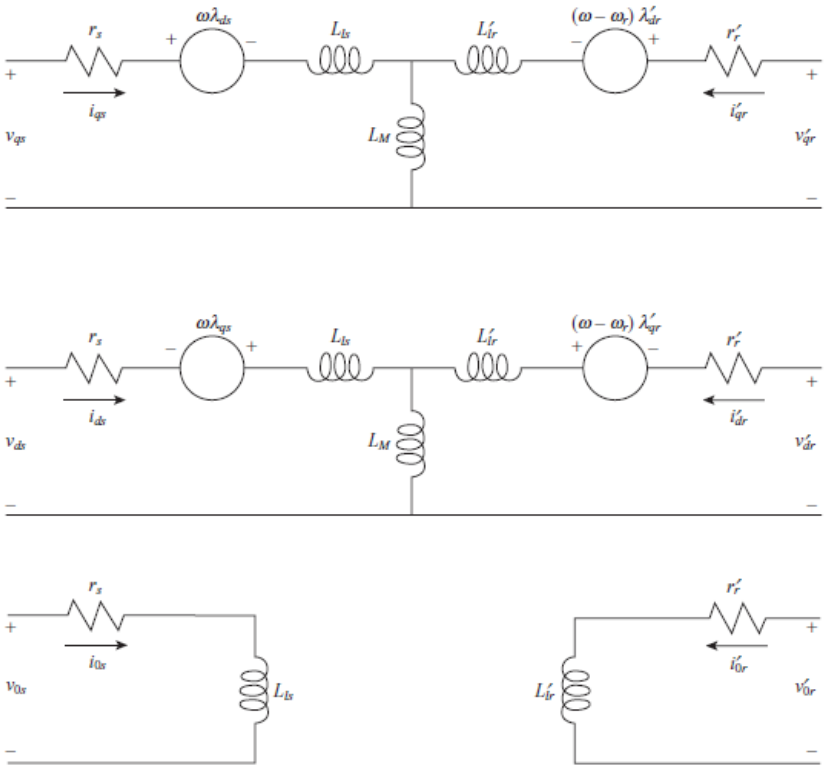

Figure 9: DQ Circuit of Three-Phase Induction Motor [17][6]

From the circuits above, the differential equations below are derived. In this new system and reference frame, the inductances are no longer dependent on the position of the rotor (θr). This allows for easier solutions, especially for dynamic responses.

[6] *Reprinted with permission from *Analysis of Electric Machinery and Drive Systems*, by P. Krause, O. Wasynczuk, S. Sudhoff, S. Pekarek, 2013, IEEE Press, Piscataway, NJ. Copyright 2013 by IEEE, Inc.

Stator Equations:

$$v_{qs} = r_s i_{qs} + \frac{d}{dt}\lambda_{qs} + \omega\lambda_{ds} \tag{3.14}$$

$$v_{ds} = r_s i_{ds} + \frac{d}{dt}\lambda_{ds} - \omega\lambda_{qs} \tag{3.15}$$

Rotor Equations:

$$0 = r'_r i'_{qr} + \frac{d}{dt}\lambda'_{qr} + (\omega - \omega_r)\lambda'_{dr} \tag{3.16}$$

$$0 = r'_r i'_{dr} + \frac{d}{dt}\lambda'_{dr} - (\omega - \omega_r)\lambda'_{qr} \tag{3.17}$$

Flux Equations:

$$\lambda_{qs} = L_s i_{qs} + L_m i'_{qr} \tag{3.18}$$

$$\lambda_{ds} = L_s i_{ds} + L_m i'_{dr} \tag{3.19}$$

$$\lambda'_{qr} = L_r i'_{qr} + L_m i_{qs} \tag{3.20}$$

$$\lambda'_{dr} = L_r i'_{dr} + L_m i_{ds} \tag{3.21}$$

$$L_s = L_{ls} + L_m \tag{3.22}$$

$$L'_r = L'_{lr} + L_m \tag{3.23}$$

Torque Equation:

$$T_e = \frac{3}{2}\frac{p}{2}(\lambda_{ds} i_{qs} - \lambda_{qs} i_{ds}) \tag{3.24}$$

where

d/dt = time differentiation;

ω = rotating velocity of DQ reference frame;

ω_r = rotating velocity of motor rotor;

p = number of poles;

v_{qs}, v_{ds}= Q,D component of stator voltages;

i_{qs}, i_{ds}= Q,D component of stator currents;

λ_{qs}, λ_{ds} = Q,D component of stator flux;

r_s = stator resistance;

i'_{qr}, i'_{dr}= Q,D component of rotor currents;

λ'_{qr}, λ'_{dr} = Q,D component of rotor flux;

r'_r = rotor resistance;

L_m = mutual inductance;

L_{ls} = stator leakage inductance;

L'_{lr} = rotor leakage inductance;

L_s = stator inductance;

L'_r = rotor inducatance;

T_e = electromagnetic torque;

Since the power electronics that feed the motor are in the stationary reference frame, it is convenient to leave the modeled system in this reference frame. Therefore, in order to transform the modeled currents and voltages from the DQ-frame to the three-phase all that is needed is the Clark's Transformation ($\theta = 0$). Conversely, the DQ stator voltage can be obtained from the three-phase supplied voltage using the Clark's Transformation. With these quantities known, the four differential equations can be solved simultaneously. The torque and power are invariant quantities. However, the speed of the rotor is an unknown quantity in equation 3.16 and 3.17. In order to determine the

speed of the rotor an equation is required to describe the mechanical coupling between the motor and the load (in this case a vehicle).

3.4. Mechanical Coupling

The induction motor does not only operate in the electrical domain, but also the mechanical. The model in the previous section discusses the electrical components that produces torque; however, the mechanical components must also be describe to define the system. The following equations determines the rotational acceleration of the rotor. Using these formulas, the complete model, electrical and mechanical components, of the motor are given.

$$T_e = J_t \frac{d\omega_r}{dt} + B\omega_r + T_l \tag{3.25}$$

$$S_m = S_l \times N \tag{3.26}$$

$$T_m = \frac{T_w}{N \times \eta_t} \tag{3.27}$$

$$J_t = \frac{J_l}{N^2} + J_m \tag{3.28}$$

where

T_e = electromagnetic torque;

T_l = load torque;

T_w = wheel torque;

ω_r = rotor's rotational velocity;

B = rotor friction coefficient;

J_t = total inertia of system;

J_l = load inertia;

J_m = rotor inertia;

N = gear ratio;

S_m = speed of the motor;

S_l = speed of the load;

Examining (3.25), the electromagnetic torque is determined by the electrical equations that describe the motor. This is given by (3.24). The rotor fiction coefficient is often ignored due to its negligible effects, especially at lower speeds. While the load torque is determined by the resistive forces on the load, in this case the vehicle. These forces will be discussed in detail in section 4. Finally, the term for inertia is introduced. This term includes the inertia from the rotor, as well as, the vehicle. The two components can be seen in (3.28). Since the vehicle is not rotating in the driver's reference frame, this concept can be difficult to conceptualize. Regardless, the vehicle has an inertia associated with it from the motor's reference frame. This transformation from reference frames is discussed in section 4. Moreover, equation (3.28) reveals the effects of gearing on the system inertia. This is an interesting relationship that will be revisited during the design of vehicle and sizing of the motor in section 5.

3.5. Control Methods

Every motor is designed with special consideration given to its nominal operating conditions. The rated three-phase voltage and frequency should produce the desired output mechanical power. At this condition, the motor is optimized for operation. However, if an application requires a range of torques and speeds, like vehicle applications, the motor control technique must be able to achieve the desired torque at any operating speed. Furthermore, the torque response of the control should be fast enough to meet the performance demands of the application. Other important features of a control method are complexity, robustness, and efficiency. One of the major disadvantages of the IM is their difficulty to control, especially for dynamic applications. This stems from the non-linear magnetic coupling and the asynchronous nature between the stator flux and rotor. This paper will discuss common control techniques for the IM that will be simulated during the research.

3.5.1. Scalar Control – Constant V/f Control

Constant V/f control is a scalar control method based off of the steady-state model of the induction motor. The steady state, per-phase circuit for the IM is shown below.

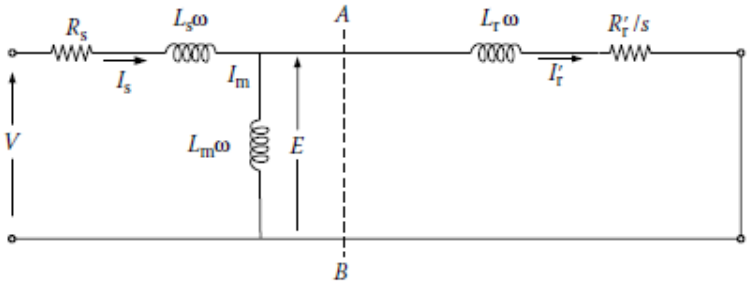

Figure 10: Steady State, Per-phase IM circuit [16][7]

The goal of constant V/f is to keep the field flux constant and at rated conditions throughout the motor's operation. This means that the current flowing through the L_m branch must be kept at rated values at all operating conditions. In order to accomplish this, the following must be met:

$$I_m = \frac{E_{rated}}{\omega_{rated} L_m} \tag{3.29}$$

It is shown in this equation that the ratio of E_{rated}/ω_{rated} must be held constant. Since the stator resistance, R_s, is typically small, the voltage drop across the resistor can be ignored at large stator voltages. This means that E_{rated} can be approximated to be the voltage applied to the stator windings. The rotor current and torque can then be calculated:

$$I'_r = \frac{(\omega/\omega_r)E_{rated}}{jL_r\omega + R'_r/s} \tag{3.30}$$

$$T_e = \frac{3}{\omega} I'_r{}^2 (R'_r/s) = \frac{3}{\omega}\left[\frac{(\omega/\omega_r)E_{rated}}{jL_r\omega + R'_r/s}\right]^2 \tag{3.31}$$

[7] *Reprinted with permission from *Modern Electric, Hybrid Electric, and Fuel Cell Vehicles*, by M.Ehsani, Y. Gao, A. Emadi, 2010, CRC Press, Boca Raton, FL. Copyright 2010 by Taylor and Francis Group, LLC

where

T_e = electromagnetic torque;

I'_r = rotor current;

ω = electrical frequency;

ω_r = rotor frequency;

E_{rated} = voltage across rotor & magnatizing branch;

L_r = rotor inductance;

R'_r = rotor resistance;

s = normalized slip;

T_e = electromagnetic torque;

Typically, the torque is the demanded quantity. With this known, the frequency can be found with the two equations and two unknowns (s, ω). Once the voltage and frequency are known, the voltage source inverter (VSI) can feed this signal to the three phases of the stator.

Often times the analytical calculations are not required to determine the input voltage and frequency. If a linear approximation is made between slip and torque, a given torque demand can determine the required slip frequency. Then, with the speed of the rotor, the stator or electrical frequency can be found. With the operating frequency obtained, the voltage magnitude can be found. Once rated voltage is reached, the voltage is held constant and the frequency increases. Since the ratio is no longer held constant, the flux decreases along with the torque, this region is commonly referred to the field-weakening region.

The block diagram describing this control is shown on the follow page.

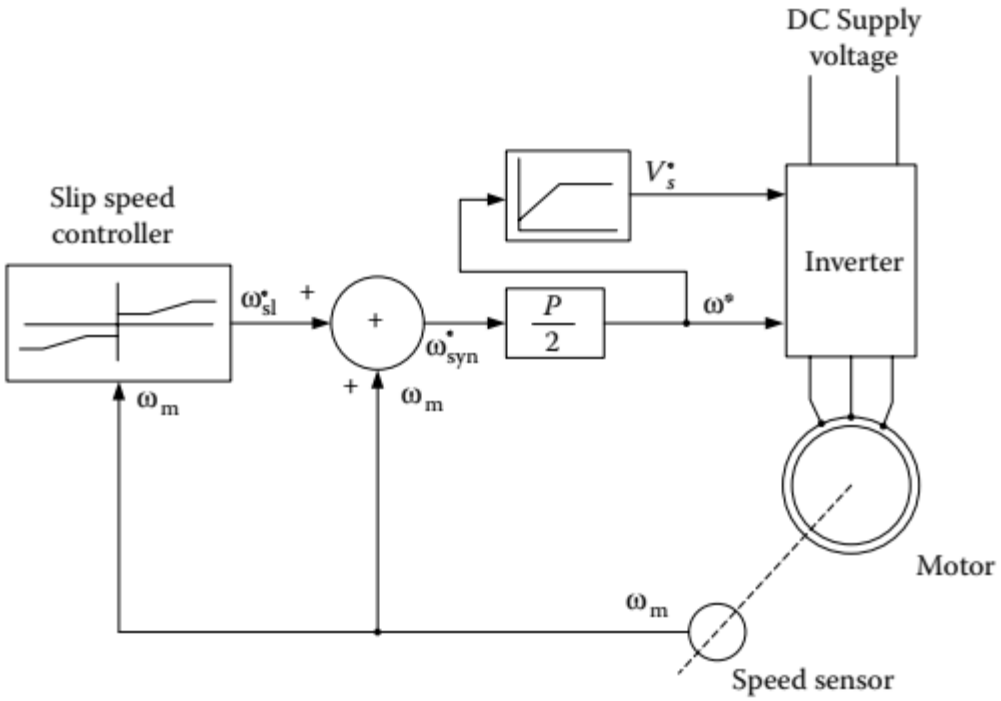

Figure 11 : Block Diagram of Closed-Loop Constant V/f [16][8]

The performance of the motor can be improved at low voltage operation by calculating the voltage drop across the stator resistance. This voltage boost allows for rated torque at low speeds. However, this control scheme is based on the steady state model and does not consider space vector position during transients, this leads to varying performance. The cause of this was discussed in section 3.1. One way to prevent this issue is to utilize a current controlled voltage source inverter to prevent the DC offset. This effect and solution will be shown in the results section. The next section provides a scalar control method that exploits this inverter control method. For the remainder of this study, scalar VSI control will refer to the previously discussed constant V/f control.

[8] *Reprinted with permission from *Modern Electric, Hybrid Electric, and Fuel Cell Vehicles*, by M.Ehsani, Y. Gao, A. Emadi, 2010, CRC Press, Boca Raton, FL. Copyright 2010 by Taylor and Francis Group, LLC

3.5.2. Scalar Control – Current Control

According to the scalar method discussed above, in order to start the IM from zero speed, the three-phase voltage is applied at low frequency (slip frequency). This application of voltage to the highly inductive circuit of the IM causes a DC voltage offset. This offset, in turn, creates a DC current and a DC flux component. Until this DC component decays, there is a torque oscillation associated with the stator DC flux and the rotor's rotating flux. This causes torque oscillation at the start of the motor that will be shown in the results section. One way to ensure there is no DC current component is to implement a current controlled voltage source inverter (CC-VSI).

A CC-VSI takes a reference AC current to the stator and compares it to the measured values in each phase of the motor windings. Then a type of hysteresis control is used to implement the CC-VSI. A hysteresis band is placed around the reference current and the motor current is kept within that band. The current is controlled by either suppling a positive or negative voltage to the motor. The outcome is illustrated in the figure below:

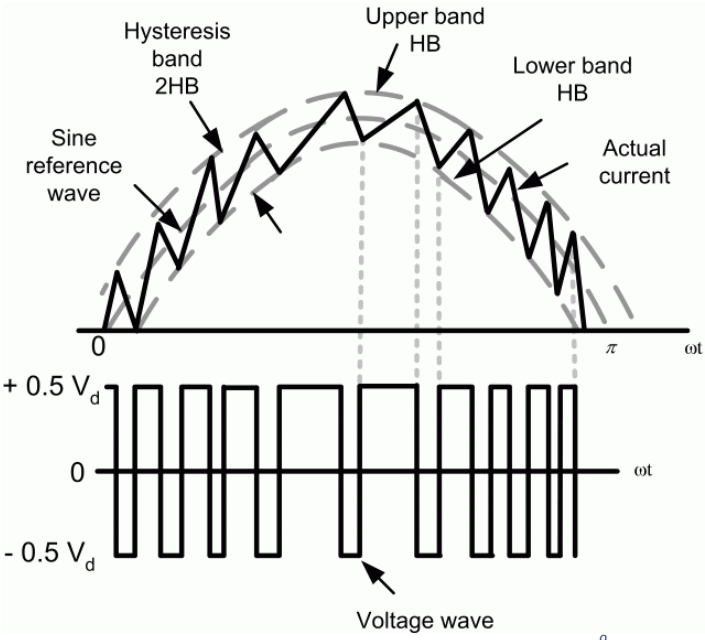

Figure 12 : Hysteresis Control of Stator Current [18][9]

When using a CC-VSI, the stator resistance and inductance can be ignored, because the inverter produces the current I_s regardless of the values of these parameters. This simplifies the steady state IM circuit model given in Figure 10. In order to simplify the calculation further, the rotor inductance can be ignored. This approximation is appropriate because the size of the magnetizing inductance is typically an order of magnitude larger than the rotor leakage inductance. Additionally, for high efficiency IM, the motor is operated at low slip resulting in a large Rr/s resistance. With this assumption, the CC-VSI fed IM circuit model becomes:

[9] *Reprinted with permission from *Simulate an AC Motor Drive*, MathWorks. Available: https://www.mathworks.com/help/phymod/sps/powersys/ug/simulating-an-ac-motor-drive.html

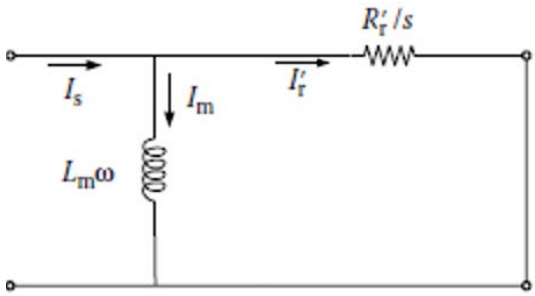

Figure 13 : Simplified IM Circuit

In order to produce the desired torque for all operating conditions, the correct stator current magnitude and frequency needs to be delivered to the CC-VSI. These parameters can be determined by utilizing the linear relationship between torque and slip, as well as, the relationship between torque and rotor current. These relationships are shown below:

$$T_e = \frac{3}{\omega_{slip}} {I'_r}^2 (R'_r/s) \tag{3.32}$$

$$I'_r = \sqrt{\frac{T_e * \omega_{slip}}{3 * (R'_r/s)}} \tag{3.33}$$

$$I_s^2 = I_m^2 + {I'_r}^2 \tag{3.34}$$

where

T_e = electromagnetic torque;

I'_r = rotor current;

ω_{slip} = slip frequency;

R'_r = rotor resistance;

I_s = stator current;

I_m = magnetizing current;

With the demanded torque value, the slip can be found using the linear relationship. Once the slip and torque are known, the rotor current can be determined. In order to define the stator current, the magnetizing current needs to be found. Since, during the operation of constant V/f, this current is kept constant at rated conditions, the value for magnetizing current can be found empirically or analytical at rated conditions. Then, using (3.34), the stator current can be found. In the remainder of this paper, this control method will be referred to as scalar CC-VSI control.

3.5.3. Vector Control – Indirect Field Oriented Control

Field Oriented Control (FOC) is one of the commonly used controls that fall under vector control. The goal of FOC is to keep the stator and rotor flux in quadrature as to always produce the maximum torque per amp. This can be accomplished even during transients and dynamic operations. Since the squirrel-cage induction motor does not have any access to the rotor flux directly, FOC utilizes the DQ transformation in order to decouple the rotor flux and torque.

As discussed in section 3.3, the DQ transformation simplifies the relationship between rotor and stator inductances. This transformation removes any dependence on the rotor position from the inductances and, therefore, greatly reduces the complexity of the differential equations. There is an additional advantage to this transformation. Using a Park's Transform, the reference frame can be rotated at any arbitrate speed. The vector diagram below shows the difference between a synchronously rotating and stationary reference frame.

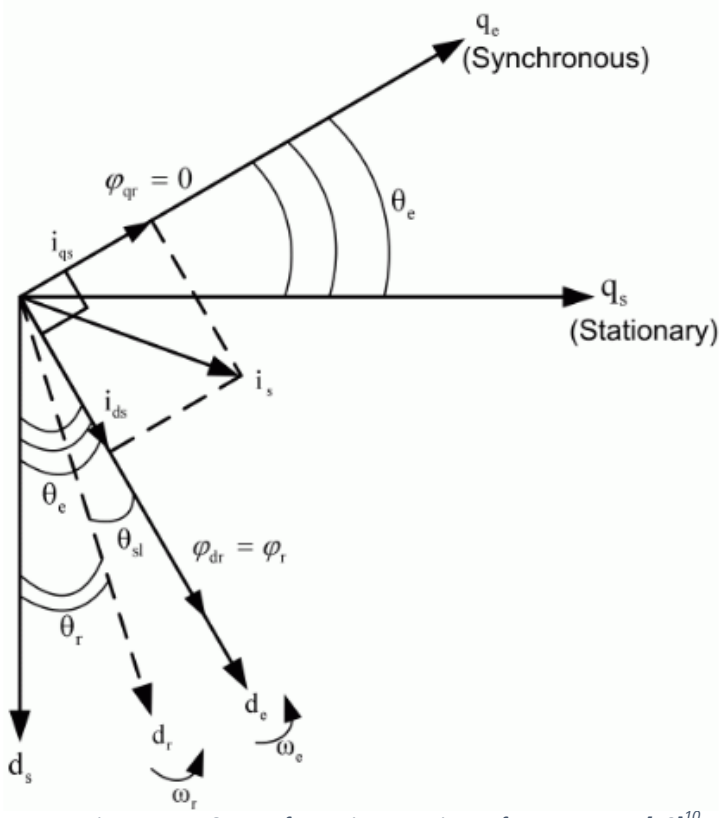

Figure 14 : DQ Transformation Rotating Reference Frame [18][10]

With the reference frame rotating, the rotor flux, φ_r, can be aligned with the d-axis as shown in Figure 14. This eliminates the second component in the torque, shown in (3.24). With the second component eliminated, the torque equation is left with the q-component of current and the d-component of flux linkage. By rotating the reference frame at synchronous speed, the torque and flux have been decoupled. This decoupling is shown in the following equations:

[10] *Reprinted with permission from *Simulate an AC Motor Drive*, MathWorks. Available: https://www.mathworks.com/help/phymod/sps/powersys/ug/simulating-an-ac-motor-drive.html

$$\omega_{sl} = \omega_s - \omega_m = \left(\frac{L_m R'_r}{\lambda^e{}_r L_r}\right) i^e{}_{qs} \tag{3.35}$$

$$\frac{d}{dt}\lambda^e{}_r = -\left(\frac{R'_r}{L_r}\right)\lambda^e{}_r + \left(\frac{L_m R'_r}{L_r}\right) i^e{}_{ds} \tag{3.36}$$

where

ω_s = electrical frequency;

ω_{sl} = slip frequency;

ω_m = mechanical or rotor frequency;

L_r = rotor inductance;

L_m = magnetizing inductance;

R'_r = rotor resistance;

$\lambda^e{}_r$= synchronous rotor flux;

$i^e{}_{qs}$= synchronous Q component of stator current;

$i^e{}_{ds}$= synchronous D component of stator current;

The rotor position can be determined by taking the integral ω_s from (3.35). This quantity is needed in order to convert commanded values of $i^e{}_{ds}$ & $i^e{}_{qs}$ from DC values in the synchronous frame to AC values in the stationary reference frame. Finally, the stationary virtual two-phase currents, i_{qds}, need to be converted back into the three-phase values in order to feed the demanded value to the CC-VSI.

This presents one of the challenges of FOC, an accurate knowledge of the rotor flux position is required in order to do the transformation from the synchronous DQ reference frame to the three-phase stationary reference frame. There are two ways to determine the position: direct or indirect. Direct requires sensors to find the rotor flux in the airgap. However, this adds expense and reduced the overall robustness of the control.

Indirect uses (3.35) to calculate the rotor flux position. This method also has challenges, as the rotor resistance can vary with temperature and age of the motor. This parameter dependence adds complexity to the control, manufacturing, and life-time services of the motor.

Now that the theory of the motor has been discussed, a detailed look at the load/vehicle will be given. This will allow for an accurate model of the entire system to by simulated to give results in context of vehicle application.

4. VEHICLE DYNAMICS

An important part of replicating the performance of a control method is modeling the load. Vehicles are complex systems. However, the system can be simplified without compromising accuracy. The mechanical coupling equations, (3.25), shown in the previous section reveals that the vehicle interfaces with the motor in two ways. The inertia of the vehicle and the external forces on the vehicle that present themselves as load torque.

4.1. Vehicle Resistances

The load torque on the motor stems from the resistive forces felt on the vehicle during a drive cycle. These resistive forces can be put in three categories: rolling resistance, aerodynamic drag, and grading resistance. These forces are illustrated in the figure below:

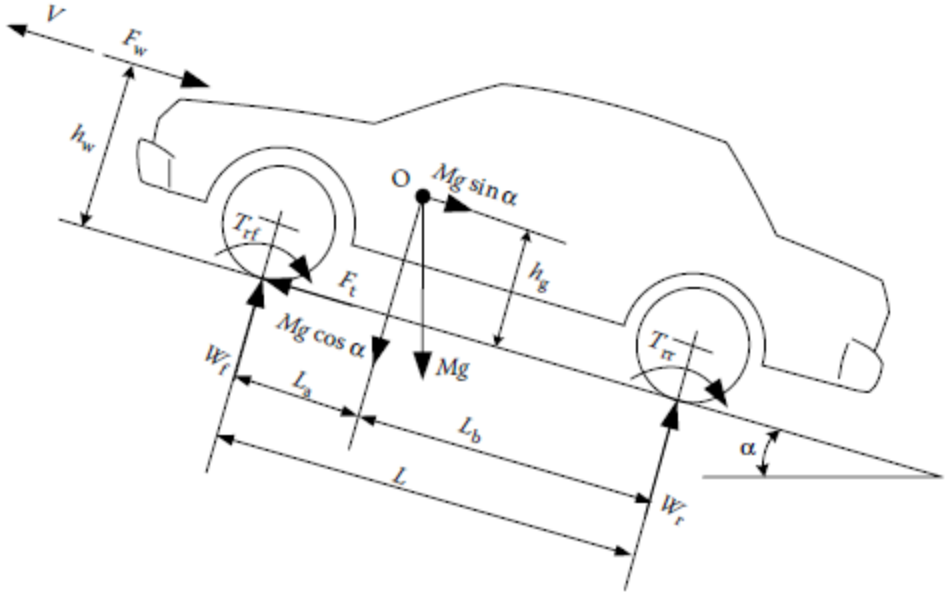

Figure 15 : Force Diagram on Vehicle [16][11]

These forces are expressed mathematically as follows:

Grading Resistance:

$$F_g = Mgsin(\alpha) \tag{4.1}$$

Rolling Resistance:

$$F_{rf} + F_{ff} = Mgf_r cos(\alpha) \tag{4.2}$$

Aerodynamic Drag:

$$F_w = \frac{1}{2}\rho_a C_D A_f V^2 \tag{4.3}$$

[11] *Reprinted with permission from *Modern Electric, Hybrid Electric, and Fuel Cell Vehicles*, by M.Ehsani, Y. Gao, A. Emadi, 2010, CRC Press, Boca Raton, FL. Copyright 2010 by Taylor and Francis Group, LLC

where

F_g = grade force;

M = total mass of vehicle;

g = acceleration due to gravity;

F_{rf} = rear tire friction force;

F_{ff} = front tire friction force;

f_r = friction resistance coefficient;

α = angle of incline of road;

F_w = aerodynamic drag force;

ρ_a = density of air;

C_D = aerodynamic coefficient;

A_f = front area of vehicle;

V = speed of vehicle;

With these forces, the load torque on the rotor shaft can be calculated. This is an important distinction from much of the literature in this area. Many of the simulations in this area use step load torques to examine the performance of the control method, however, the resistive forces shown above happen gradually and not as an instantaneous step with the expectation of a steep incline.

4.2. Inertia, Mass, & Dynamic Equations

With knowledge of the external forces on the vehicle, the only unknown left in equation (3.25) is the inertia (this is neglecting the viscous friction of the bearings). The motor and vehicle operate in two different reference frames: rotational and translational. The rotational reference frame is natural from the motor's perspective, but the translational mass and forces of the vehicle must be converted to this reference frame. On the other hand, the translational reference frame is logical from the vehicle's

perspective, but the motor's torque and inertia need to be converted to the translational reference frame. In order to verify the accuracy of the assumptions made during the conversions of the masses, inertias, torques, and forces; both transformations were carried out to ensure the same results were produced.

4.2.1. Rotational Reference Frame

As mentioned previously, the dynamic/coupling equation in the rotation frame is given below:

$$T_e = J_t \frac{d\omega_r}{dt} + B\omega_r + T_l \tag{4.4}$$

$$J_t = \frac{J_v}{N^2} + J_m \tag{4.5}$$

where

T_e = electromagnetic torque;
T_l = load torque;
ω_r = rotor's rotational velocity;
B = rotor friction coefficient;
J_t = total inertia of system;
J_v = vehicle inertia;
J_m = rotor inertia;
N = gear ratio;

The inertia consists of two components, the rotor and the vehicle. In order to determine the inertia of a vehicle, complex machines called Vehicle Inertia Measuring Machines (VIMM) are used. These machines determine the inertia of the vehicle in ever dimension. For this research, the vehicle mass will be simplified to find an appropriate

approximation for the inertia without the complexity of the VIMM. The vehicle can be approximated by a mass on a conveyer belt shown below.

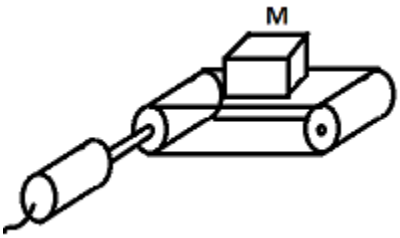

Figure 16: Simplified Vehicle Inertia

If the inertia of the pulley and belt are ignored, the inertia of the vehicle can be approximated by the following:

$$J_v = MR^2 \tag{4.6}$$

where

M = mass of the vehicle;

J_v = vehicle inertia;

R = radius of the wheel;

In reality, the inertia of the vehicle has X, Y, Z components that differ due to the asymmetry of the system. However, for this simulation, the only motion considered is in a single plane, the direction of movement. This simplification is appropriate for this study because this motion determines, in general, the performance of the motor.

With the inertia determined, the only unknown left in (4.4) is the load torque. This can be found using the forces in section 4.1 and converting them to torque. To do this, the forces are multiplied by the radius of the wheel.

4.2.2. Translational Reference Frame

Using the forces mentioned in section 4.1, the dynamics of the vehicle could be determined using Newton's second law of motion. The summations of the forces consist of the tractive effort on the tires, F_t , and resistive forces, F_r. The tractive effort force, generated by the motor, is found using (3.27) and dividing the motor torque by the radius of the wheel. The resistive forces were listed in section 4.1. With these forces, Newton's second law can be expressed as follows:

$$\frac{dV}{dt} = \frac{\sum F_t - \sum F_r}{\delta M} \tag{4.7}$$

$$\delta M \frac{dV}{dt} = \left(F_{tf} + F_{tr}\right) - \left(F_{rf} + F_{ff} + F_w + F_g\right) \tag{4.8}$$

$$\delta = 1 + \frac{I_W}{Mr_d^2} + \frac{i_0^2 i_g^2 I_p}{Mr^2} \tag{4.9}$$

$$\delta = 1 + \delta_1 + i_0^2 i_g^2 \delta_2 \tag{4.10}$$

$$T_w = i_g i_0 \eta_t T_p \tag{4.11}$$

$$F_t = \frac{T_w}{r_d} \tag{4.12}$$

where

F_t = tractive effort;

F_r = resistive forces;

F_g = grade force;

M = total mass of vehicle;

F_{rf} = rear tire friction force;

F_{ff} = front tire friction force;

F_{tr} = rear tire tractive effort;

F_{tf} = front tire tractive effort;

F_w = aerodynamic drag force;

δ = total mass factor;

i_o = fixed gear ratio;

i_g = transmission gear ratio;

I_w = total angular inertial moment of the wheel;

I_p = total angular inertial moment of rotating components of the power plant;

r = rotor radius;

r_d = wheel radius;

δ_1 = wheel mass factor;

δ_2 = power plant mass factor;

η_t = transmission efficiency;

T_p = power plant torque;

T_W = wheel torque;

The equations introduce a new term called mass factor, δ. This factor accounts for additional mass associated with the inertia of the rotational components of the vehicle: the wheels and rotor. The second component in (4.9) & (4.10) relate to the wheels, while the third component corresponds to the rotor. From the mass factor equation, it can be seen that the fixed gear ratio plays an important role in the inertia seen by the system. This design parameter is considered in the next section when designing the motor and vehicle.

5. ELECTRIC VEHICLE DESIGN

The equations in the previous section can be used to evaluate the driving performance of a vehicle; however, realistic values need to be assigned to the model to mimic a common passenger vehicle. Acceleration and top speed of the vehicle need to be dictated to determine the size/power rating of the motor. In this paper, the battery and power electronics will not be considered. Although these components are important design parameters in EVs, the focus of this research will be on the control method, motor, and vehicle performance.

The steps to define the vehicle and motor are as follows:

1. Choose Vehicle and Performance Parameters
2. Choose Fixed Gear Ratio
3. Determine Motor Power Rating

The next three sections will show these steps in detail. Once the parameters are well defined, the model and controls can be built for the simulation.

5.1. Vehicle Parameters

First, environmental, vehicle, and performance parameters must be defined. The following values for this vehicle have been borrowed from reference book [16] by Dr. Ehsani.

Vehicle Parameters	
Vehicle Mass	1500 kg
Rolling Resistance Coefficient (f_r)	0.01
Aerodynamic Drag Coefficient (C_D)	0.3
Front Area (A_f)	2.0 m^2
Radius of Wheel	0.3 m
Transmission Efficiency (Single Gear)	0.9
Mass Factor- Wheel Component (δ_1)	0.04
Mass Factor- Rotor Component (δ_2)	0.0025

Table 1: Vehicle Parameters

Environmental Parameters	
Gravity	9.81 m/s^2
Density of Air	1.205 kg/m^3
Road Slope	0°

Table 2 : Environmental Parameters

Performance Parameters	
Top Speed	160 km/h
Acceleration	2.78 m/s^2

Table 3 : Performance Parameters

Using these parameters and the forces described in section 4, the required motor power can be found for the maximum acceleration parameter in Table 3. This power requirement can be used to find the rated torque for the motor.

$$P_m = \frac{V}{1000\,\eta_t}\left(Mgf_r cos(\alpha) + \frac{1}{2}\rho_a C_D A_f V^2 + Mgsin(\alpha) + \delta M\frac{dV}{dt}\right) \qquad (5.1)$$

where

M = total mass of vehicle;

g = acceleration due to gravity;

f_r = friction resistance coefficient;

α = angle of incline of road;

ρ_a = density of air;

C_D = aerodynamic coefficient;

A_f = front area of vehicle;

V = speed of vehicle;

η_t = transmission efficiency;

δ = mass factor;

P_m = motor power;

However, there is one unknown in the (5.1). The equation has the mass factor constant in the last term. The equation for the mass factor is shown in section 4.2.2, (4.9) and (4.10). It is shown in these equations; the mass factor depends on the gear ratio. The gear ratio needs to be found before the motor size can be found.

5.2. Design of Gearing

Consider a motor of a given power capacity. Since power is the product of speed and torque, a motor can deliver a given power to a load using high torque/low speed or low torque/high speed. High-speed motors have several advantages over high torque, such as, smaller physical size and higher efficiency. These are attractive characteristics for traction motors, so it is common practice to have the motor run at high speeds and gear down to vehicle speed.

Nevertheless, the gear ratio cannot be exceedingly high. Equations (4.9) and (4.10) reveal that the mass factor has terms for the vehicle, wheels, and rotor. With a gear ratio of one, the rotor term is small compared to the mass of the vehicle. This is because there is little energy stored in a slow spinning rotor. However, as the gear ratio increases, this component grows and becomes significant. It is important to have a high gear ratio that minimizes physical size, as well as, improve efficiency, but this must be accomplished without having to increasing the motor's power capacity significantly.

Using the constraint of the acceleration of the vehicle (2.78 m/s^2), the rated traction power and rated torque can be found for a variety of gear ratios. The figure below reveals an interesting relationship. As the gear ratio increases, the required rated torque decreases while asymptotically approaching a lower limit. Additionally, the rated speed of the motor increases with the gear ratio, since the torque is no longer decreasing, the rated power increases.

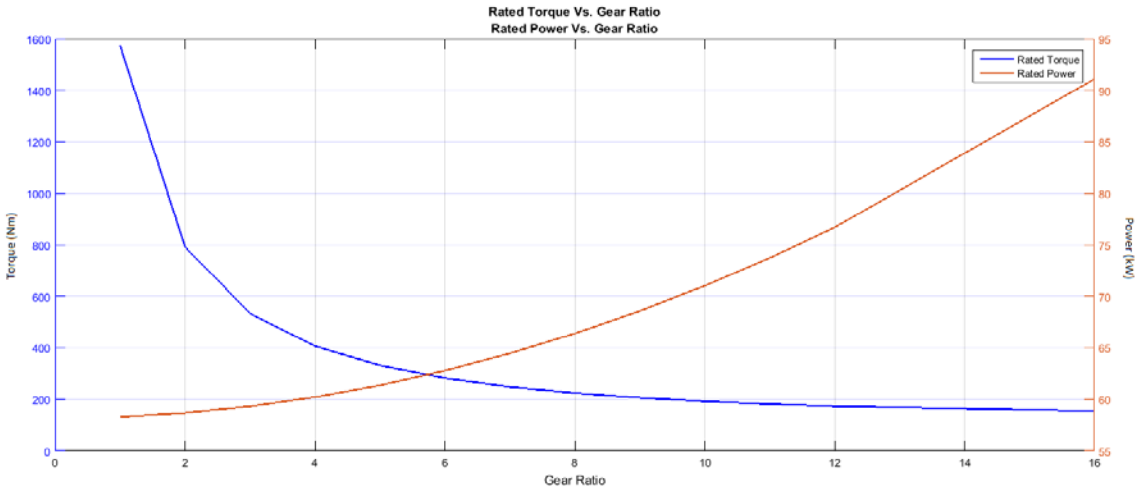

Figure 17 : Rated Torque/Power versus Gear Ratio

From this graph, a reasonable gear ratio can be anywhere between 6 and 12 depending on the application and motor design. Choosing the correct gear ratio in this range would require optimizing the entire system including: the battery, power electronics, motor, and gear box. This subject would require further research. For brevity, choosing a gear ratio in the middle of this range will suffice. The power rating

has not been significantly increased and it agrees with the ratios seen in the industry. The gear ratio for this simulation will be the following:

Gear Ratio
10: 1

Table 4 : Gear Ratio

5.3. Design of the Motor

With the gear ratio known, the traction motor can be defined. The maximum speed for the vehicle was selected to be 160 Km/h. Since the radius of the wheel is 0.3 m, this corresponds to a maximum RPM for the vehicle wheel of 1414.7 RPMs. Therefore, the maximum speed of this high-speed induction motor is 14,147 RPMs. In Ehsani's book, [16], the speed ratio of a motor is defined. This ratio of maximum speed and rated speed determines how long the field weakening or constant power region of a motor extends.

$$x = \frac{maximum\ speed}{rated\ speed} \tag{5.2}$$

The speed ratio for an induction motor is approximately four according to [16]. This means that the rated speed of the motor required for this vehicle is 3,536 RPMs. From the acceleration requirement dictated in Table 3, (5.1) can be used to find the rated torque: ~172 Nm.

Accurate parameters for custom designed motor, such as this, are not open to the public. Simulink has a catalog of machines under their SimPowerSystems library. In these blocks, a number of different sized motors are given with their parameter values. These machines are industry standard machines with rated speeds of about 1,700 RPM. Selecting the motor with the appropriate rated torque is a strategy used to mimic this custom motor. In order to simulate a high-speed motor, a higher frequency and voltage

will be feed to the motor to meet the desired high-speed profile. However, there would need to be added insolation and high-quality bearings for the high-speed motor. These changes should not affect the parameters of the motor drastically. Using this approximation, the 50 HP motor with a 200 Nm rated torque was selected to represent the high-speed motor. The complete parameters for the simulated motor (with the parameters taken from the 50 HP motor) are given in the table below.

Motor Parameters	
Stator Resistance (R_s)	0.09871 Ω
Rotor Resistance (R_r)	0.1081 Ω
Mutual Inductance (L_m)	0.04717 H
Stator Leakage Inductance (L_{ls})	0.001245 H
Rotor Leakage Inductance (L_{lr})	0.001245 H
Rated Voltage	575 V
Rated Speed	3,536 RPM
Rated Current	~64 A peak
Rated Torque	172 Nm
Rated Power	64 kW
Number of Poles	4

Table 5 : Motor Parameters

In the next section, these parameters will be utilized in order to model the induction motor of the electric vehicle.

6. SIMULATION BUILD

In order to simulate the electric vehicle, both mechanical and electrical fields must be modeled. Matlab/Simulink is a powerful environment capable of achieving this multidisciplinary simulation. The interface between Matlab and Simulink is seamless; this allows the utilization of both tools during the simulation, leveraging their strengths.

6.1. Matlab Environment

The strengths of Matlab lie in data set operations. Matlab is a workspace that uses its proprietary programming language in order to manipulate matrices, plot functions, and implement algorithms. The language is similar to other object-oriented computer programming languages. During this research, the Matlab environment was used to determine the size of the motor and the load torque associated with the vehicle dynamics. The steps to find the size of the motor were given in the previous section. Matlab was also used to find the forces acting on the vehicle during a realistic drive cycle, the FTP-75 Urban Drive Cycle.

6.1.1. Drive Cycle

While reviewing the literature in this area, the common motives for not implementing a scalar control were low speed performance and slow dynamic torque response. In order to test these two qualities of the control, an appropriate drive cycle must be selected. City driving requires slow speed, as well as, many acceleration/deceleration cycles making it a suitable profile to test these conditions. A

standardized speed profile is available for such a drive cycle called the FTP-75 urban drive cycle.

MathWorks provides a ‘block’ that outputs the speed and acceleration profile of the FTP-75 urban drive cycle. This block gives a data point every second of the cycle for the thirty-minute drive. In order to make the data set continuous, Matlab interpolated between each data point. The following profiles were generated from Matlab and Mathworks’ block.

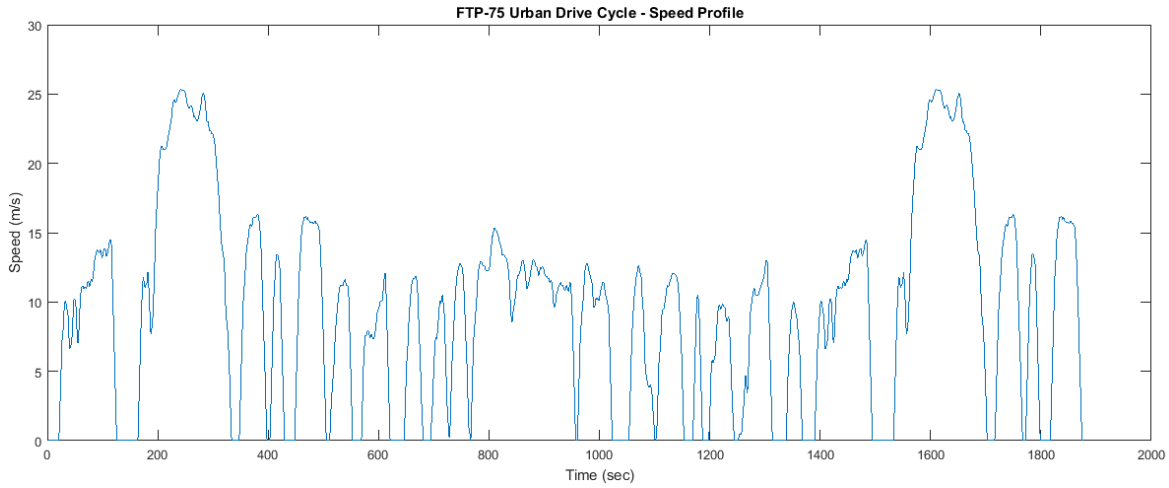

Figure 18 : FTP Speed Profile

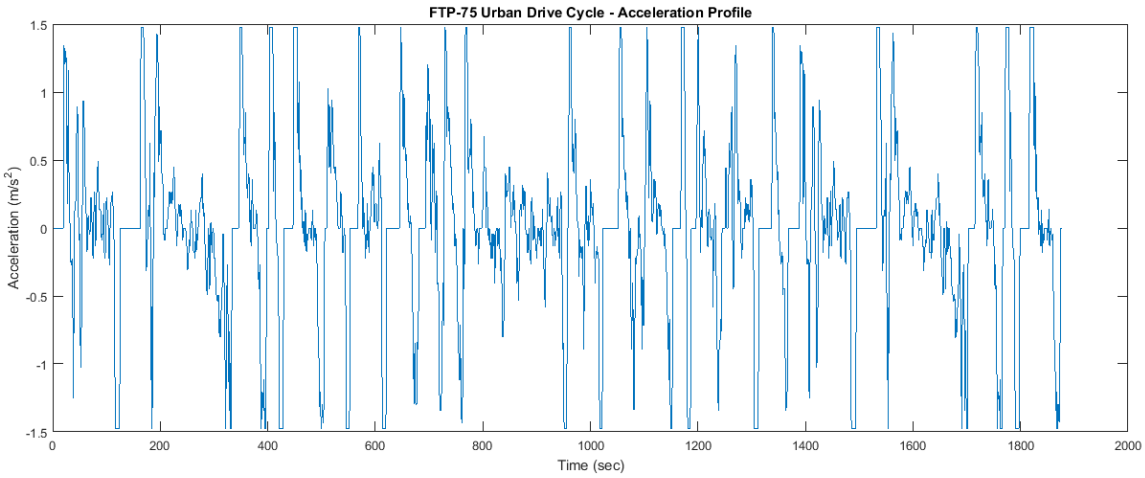

Figure 19 : FTP Acceleration Profile

Using these values, the instantaneous values for the forces on the vehicle and subsequent load torque can be found. The forces can be found with the equations giving in section 4. The torque required to accelerate the vehicle will be found using a closed speed loop and a PI controller in Simulink (discussed in section 6.2). The FTP drive cycle does not account for hills, so the forces due to grade level are ignored. This leaves two forces: tire friction and air resistance. These forces can be given it terms of torque on the wheels of the vehicle. The result is shown in the resistive torque profile below.

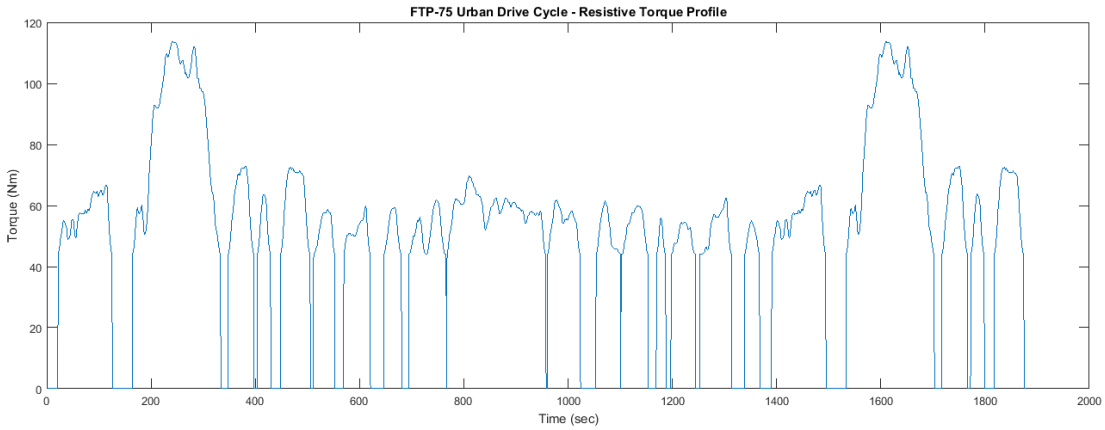

Figure 20 : Resistive Torque Profile

As expected, the load torque profile is similar to that of the speed profile. The friction force from the tires adds a small constant torque on the wheel, while the air resistance force is proportional to the velocity squared. Once the forces are found, they will be fed to the Simulink environment. During the simulation, the load torque will be used in the mechanical coupling equation to determine the speed of the motor's rotor. This constraint on the motor's speed is an important physical restraint for traction applications. The type of vehicle load torque is different than the typical step torques applied to the motors in existing literature in this area.

6.1.2. Limitations

The Matlab & MathWorks FTP75 'block' has one major limitation. As mentioned earlier, since the block only generates data points every second, Matlab must interpolate the data points. This allows Simulink with a smaller time steps to utilize the FTP data with the large time steps. But, this produces discrete steps in the change of speed of the vehicle. Since the slope of the speed changes instantly at these one second intervals, the

demanded torque will change instantly at one second intervals. This is analogous to the vehicle pedal reading in torque demands every second. This is not a realistic frequency for the input of the pedal. Instead, it is expected that the pedal input would be read frequently, 1000's of times per second. This would lead to gradual changes of torque (associated with the driver's slow moving foot) versus sharp discrete changes every second. This limitation is acceptable for this research because it shows the worst-case scenario for scalar control. If the performance of the vehicle is still not significantly degraded while running the simulation with this low fidelity torque demand, it can be concluded for a higher fidelity that the performance would be improved for the scalar control. This limitation will be revisited during the discussion of the results in the next section.

6.2. Simulink Environment

Simulink is a graphical interface that utilizes block diagrams in order to model complex systems. The block diagram environment makes for an especially powerful tool for simulating feedback/control loops. The Simulink diagram for this research can be broken down into three main components: the induction motor model, the control logic, and the vehicle/load dynamics.

6.2.1. Induction Motor Model

While scalar control uses the steady-state IM model to determine the input voltage and frequency, it is important that the IM model that is simulated is a dynamic model. Therefore, the effects of using a steady-state based control will be seen for a realistic dynamic system. As was shown in section 3, the four differential equations in the DQ

reference frame that are used to describe the dynamics of the IM are (3.14), (3.15), (3.16), and (3.17). The Simulink model is made using these four differential equations. Since the model utilizes the DQ reference frame, the physical signals in the stationary three-phase reference frame must be transformed before being fed to the IM model. The model is given a two-phase voltage in the stationary DQ reference frame, along with the speed of the rotor from an electrical perspective (multiplied by the number of poles). With the voltage and speed of the rotor known, the DQ currents are found in the stator and rotor. The relationships for flux and torque are given by (3.18), (3.19), (3.20), (3.21), and (3.24), and are used to find the remaining quantities of the motor. Once all variables are known, the quantities can be transformed back into the stationary three-phase reference frame. These are the physical signals of the system. The developed torque of the motor is invariant. On the next page, the block diagram for this induction motor is shown. The differential equations each have a subsystem that contains the algebra from the equations in section 3. In order to solve these differential questions in Simulink, a time step of 2e-06 seconds was needed.

The parameters for the induction motor were borrowed from the SimPower Systems model that is built into Simulink given in Table 5.

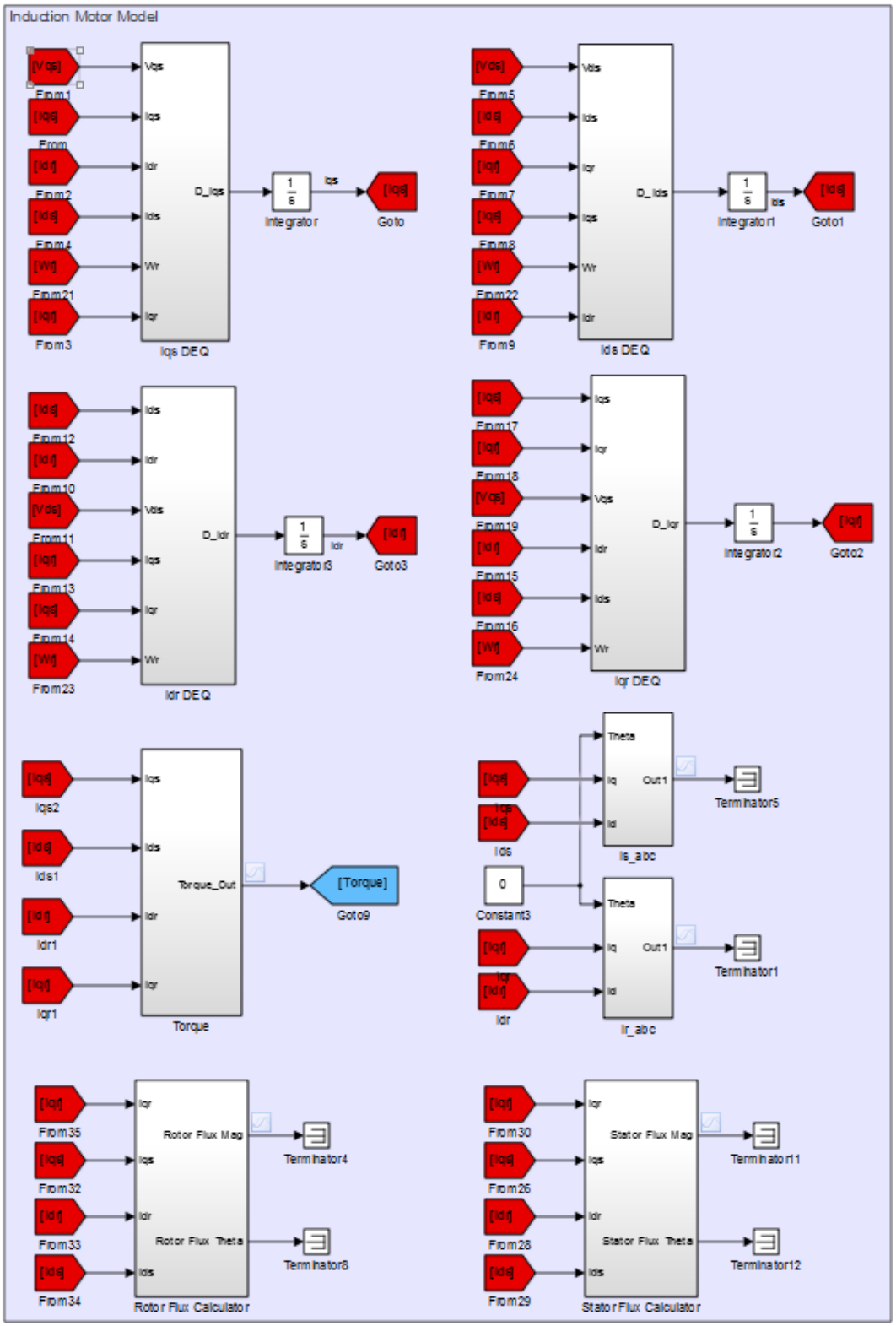

Figure 21 : Induction Motor Block Diagram

6.2.2. Control Loop

In a vehicle, the driver demands a torque to achieve a desired speed. In this simulation, a PI controller is used in place of the driver. As mentioned previously, the FTP-75 urban drive cycle is used to mimic the realistic speed demands of a vehicle. The PI controller tracks this reference speed profile. This aspect of the simulation incorporates both the driver's behavior and the pedal sensitivity. These factors are difficult to simulate as they differ from vehicle to vehicle and driver to driver. However, there is substantial flexibility in the pedal input. When driving different cars, people will notice the different sensitivity to the response of various vehicle pedals. A lot of work goes into how the vehicle responses to the acceleration pedal. The pedal responses can be complex and non-linear depending on the applications. Therefore, it is not crucial for the PI controller to be able to accurately mimic the driver's response because the pedal input qualifications can be manipulated to provide the appropriate demand to the controller.

The torque demand that comes from the PI controller, is fed to the controller. Usually, the controller than gives commands to the power electronics to control the voltage to the motor. In this simulation, there are no power electronics, the voltage is fed directly to the motor. In the case of the CC-VSI, there are ideal switches to mimic this behavior. The control loops read from left to right, ending with the transformation from the three-phase voltage to the two-phase voltage to be fed to the motor model. The three controllers utilized are Closed-loop V/f, Closed-loop Current Controlled V/f and Indirect FOC.

6.2.2.1. VSI Scalar (Closed-loop V/f)

The first control loop is based off the method outlined in section 3.5.1. The block diagram used to simulate the scalar controller with the voltage source inverter (VSI) is shown below:

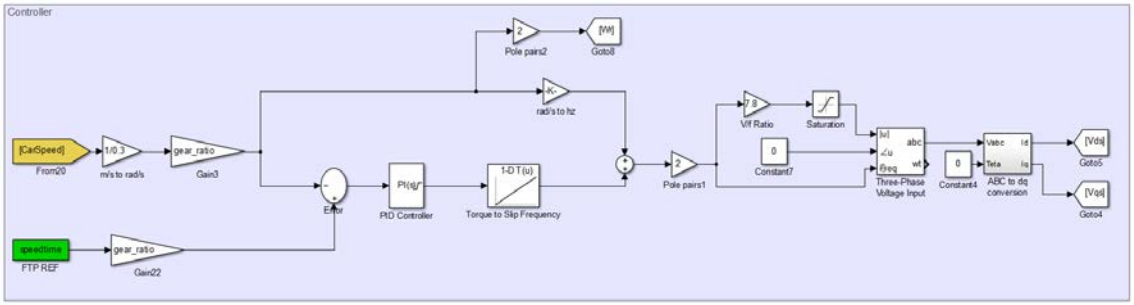

Figure 22 : VSI Scalar Block Diagram

There are four components to this block diagram. First, as mentioned earlier, the driver and pedal are simulated with a PI controller. The FTP reference speed and speed of the motor are subtracted to find an error. This error is fed to the PI controller, which outputs a torque demand. Second, the vehicle/motor speed is fed back to the controller. This closed-loop allows for accurate speed control of the motor. With the speed of the motor known, all that is required is the slip frequency. In order to find the slip frequency, the torque demand from the PI controller is used to find the slip. Since this scalar controller operates the motor at rated field flux, the linear relationship approximation between slip and torque is used. This relationship can be found empirically or theoretically. Finally, this slip frequency can be added to the mechanical

speed of the rotor (taking into consideration the number of poles) to determine the stator's electrical frequency. With this frequency, the constant V/f ratio is applied to generate the appropriate voltage. In the absences of power electronics, these values are fed to a three-phase voltage generator, which is converted into the stationary DQ reference frame to be fed to the induction motor model.

The performance of this control with some variations will be shown in the results section. Some of the variations made to the controller are a voltage boost, and a constant high slip frequency start to the motor to improve starting torque.

6.2.2.2. CC-VSI Scalar (Closed-Loop)

The current fed scalar control has some performance advantages that will be revealed in the results section of this paper. The method used for this control was given in section 3.5.2. The alterations made to the block diagram can be seen in the following Simulink image.

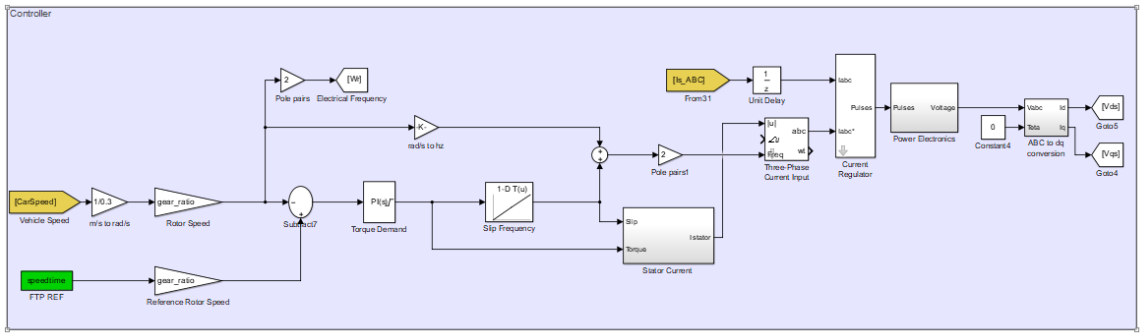

Figure 23 : CC-VSI Scalar Block Diagram

The closed-loop feedback, PI controller, and linear relationship between torque and slip frequency are all the same as the VSI scalar controller. However, the magnitude of

the stator current must be found instead of the voltage. So, the constant V/f ratio cannot be used. Instead, the simple model and equations discussed in section 3.4.1.1 are used to find the stator current amplitude. These calculations are contained in the 'Stator Current' subsystem shown on the next page.

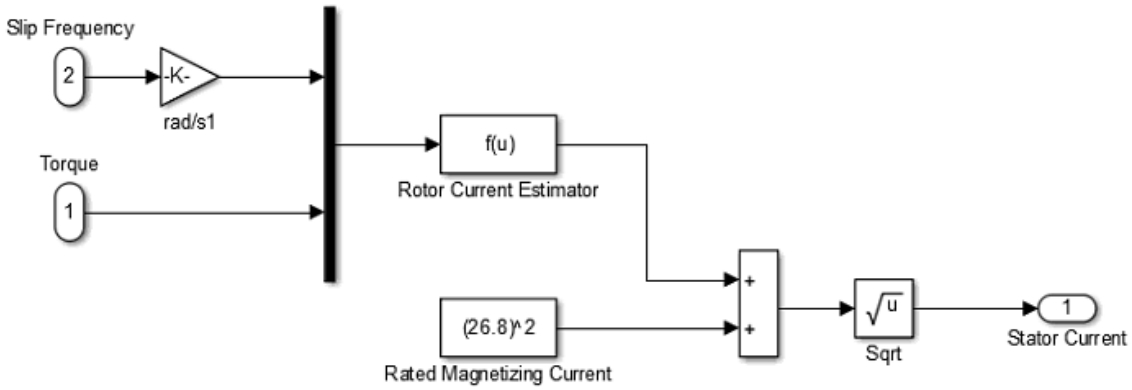

Figure 24 : 'Stator Current' Sub-Block Diagram

Assuming the rotor current and magnetizing current are in quadrature, the square of the currents can be added to find the square of the stator current. The 'Rated Magnetizing Current' can be manipulated for certain operating conditions to improve efficiency. However, if rated field flux is no long applied, the linear relationship between torque and slip is no longer valid.

Once the stator current magnitude and frequency are determined, hysteresis control is used to implement the CC-VSI. This requires a measurement of the stator current. These values are read in as 'Is_ABC' in the block diagram in Figure 23. The stator

current is compared to the reference current. A hysteresis band is placed around the reference current and the motor current is kept within that band. This control technique was discussed in section 3.5.2. As before, the signal is taken and transformed to the stationary DQ reference frame to be fed to the induction motor model. The performance of this controller will be explored in the results section.

6.2.2.3. Vector (Indirect FOC)

Indirect Field Oriented Control (IFOC) is a popular control method because it does not require any additional sensors to determine rotor flux position. The algorithm used was given in section 3.5.3. The following control loop in Simulink for IFOC:

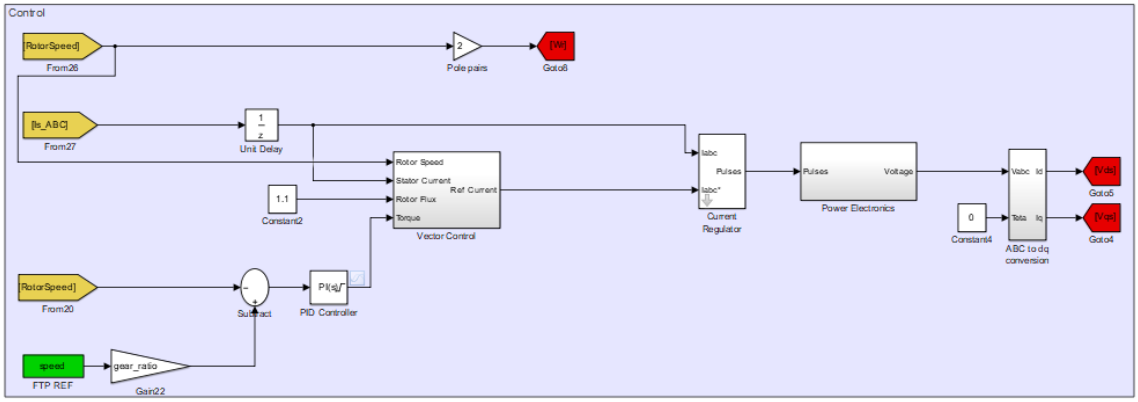

Figure 25 : Vector (IFOC) Block Diagram

The block diagram is similar to the previous two control loops. There is a reference speed and motor's speed. An error is found and a PI controller than demands the appropriate torque. The control also requires a current feedback loop because IFOC utilized a CC-VSI. The 'Vector Control' block is given the necessary inputs: Rotor

Speed, Stator Current, Rotor Flux, and Torque. For this simulation, the rotor flux is held constant at rated conditions. If efficiency were to be considered, a LMA could be used to determine the rotor flux value to maximize efficiency at the operating point. With these inputs, the vector control subsystem uses the formulas outlined in section 3.5.3 to find the reference current in the synchronous DQ reference frame. The calculations that take place inside the 'Vector Control' subsystem are given below:

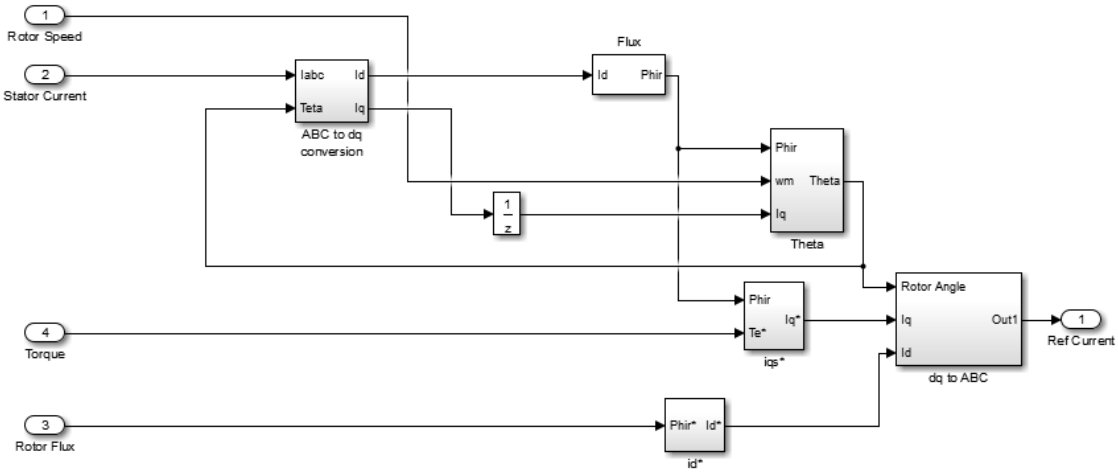

Figure 26 : 'Vector Control' Sub-system Block Diagram

Since the calculations are done in the synchronous DQ reference frame, the stator current must be transformed. This requires the position of the rotor flux (Teta). The reference values of 'd' and 'q' current components are calculated from the demanded torque and rotor flux. Finally, with an accurately calculated rotor position, the synchronous DQ values can be transformed back into the stationary three-phase

reference frame for the power electronics and motor. The additional transformations for vector control adds complexity to the controller, especially when indirectly calculating the rotor flux position via the stator currents. These calculations depend heavily on motor parameters. So, in order to reliably calculate the rotor position, information on parameter values dependence on temperature, frequency, and degradation must be well known.

The effects of the parameter changes are not considered during simulation. Instead the best case scenario is tested in order to compare the scalar to ideal performance of vector control.

6.2.3. Vehicle Dynamic Model

In section 4, the vehicle dynamics were expressed in the linear or rotation reference frame. After verifying that both reference frames yield similar results, the linear reference frame was the chosen method during simulation. Therefore, the vehicle speed was determined using Newton's equation with the addition of the mass factor. Below is the block diagram that express these equations.

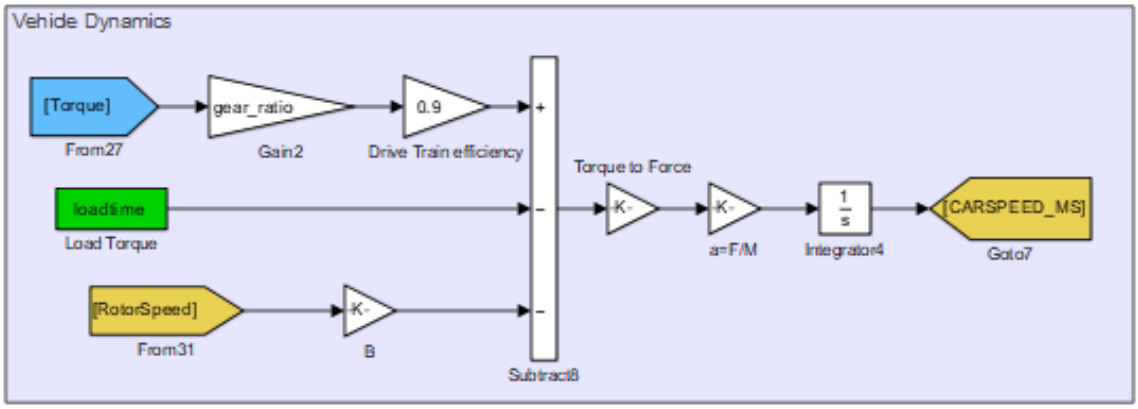

Figure 27 : Vehicle Dynamics Block Diagram

The torque shown is the electromagnetic torque produced by the motor. This torque is multiplied by the gear ratio to give the torque delivered to the wheels. There is also an additional loss associated with the gearbox. This was approximated to be 90% efficient. Then the load torque and bearing friction is subtracted from this generated torque. As mentioned in section 6.1, the load torque is calculated in Matlab prior to the simulation using the FTP-75 urban drive cycle. The load or resistive torque is fed into Simulink as a 'timeseries' data structure that syncs with the reference speed of the vehicle. The bearing friction was assumed to be small and does not play an important role in the performance difference of the two controls. Once the losses are subtracted, the torque is converted to a force and then divided by the mass of the vehicle multiplied by the mass factor (which includes the rotational inertias of the wheels and rotor). This gives the instantaneous acceleration of the vehicle. Finally, the speed of the vehicle is determined by integrating the acceleration.

The vehicle speed profile will help determine the performance of the vehicle from the driver's perspective. If the profile does not vary from that of the FTP profile, than the driver's experience will be similar regardless of the control method. This will be investigated in the results.

6.2.4. Limitations

The Simulink IM model and control loops have some limitations that prevent them from replicating some phenomenon that would present themselves in a physical system. These limitations will be identified here and then addressed in the results sections.

Explanations as to why the limitations do not affect the overall conclusions of the research will be given.

This IM model has two common simplifications. First, the model does not take into account the saturation of iron. This assumption is valid because motors are designed to run at a rated flux and below. In this region, the iron is not saturated and the relationship between current and flux is linear. Since there is no intention of operating the motor outside of the designed conditions, this is an appropriated assumption. Second, the losses in the iron caused by Eddie currents are ignored. These loses depend on the frequency of operation. As the frequency mainly depends on the speed of the wheels, it will not influence the control methods differently. This could play an important role when considering efficiency, but since that will not be done during this simulation it does not need to be incorporated into the model.

Another limitation of this Simulink model is related to simulation of the driver. The control loop utilizes the speed profile for the FTP75 drive cycle. With the error in speed between the vehicle speed and FTP75 drive cycle, the PI controller drives the motor to minimize this error. There are two issues with this model of the driver.

First, the PI controller is reactive to the reference speed of the FTP75 drive cycle. This means that time must past, an error must be created in order for the PI controller to response. While in actuality, the driver does not response in such a way. The reactive nature of the PI controller also adds a delay to the torque response of the system to the FTP75 speed profile. This artifact is justified because it creates another worst-case scenario for the performance of the controller. If the performance of the vehicle with the

controllers is seen as satisfactory, it can be concluded that the actual performance will be better.

Second, the values of the PI controller must be determined. This is a difficult value to determine because it must reflect the torque demand from the driver. This differs from driver to driver and can also be affected by the sensitivity of the pedal. Instead of attempting to capture the realistic torque demands of the driver and pedal, a PI value was selected as to allow the vector control to respond quickly. This same PI value is used for the scalar control, which leads to delayed torque response and overshoot. Any non-linear inputs from the PI (like overshoot) could be programmed into the pedal response to improve performance. This would require tuning with the vehicle. The ramifications of these limitations will be shown in the results section.

7. RESULTS

The results of the simulated system outlined in the preceding sections are discussed here. The following section provides early discoveries of the research that led to progressions in understanding and control techniques. The breath of data is provided with the procedures used to obtain the data. Preliminary observations and deductions are provided with the data analysis.

7.1. The Starting Performance

The FTP-75 drive cycle will investigate the traction motor's ability to track a dynamic scenario. Before the entirety of the drive cycle is considered, the start of the motor is of particular interest. At the start, there are many transients that take place. Since scalar controllers do not consider these transients, close attention will be paid to the performance during the start. This section will explore the starting performance for various control methods.

7.1.1. Scalar Control – Constant V/f

The first data of interest is the starting performance of the scalar VSI controller (constant V/f). The algorithm of this method was discussed in section 3.5.1 and the Simulink control loop was given in section 6.2.2.1. The simulation of constant V/f scalar control revealed poor torque control and speed response at start up. The starting torque and the subsequent speed of the vehicle is shown in the following graphs.

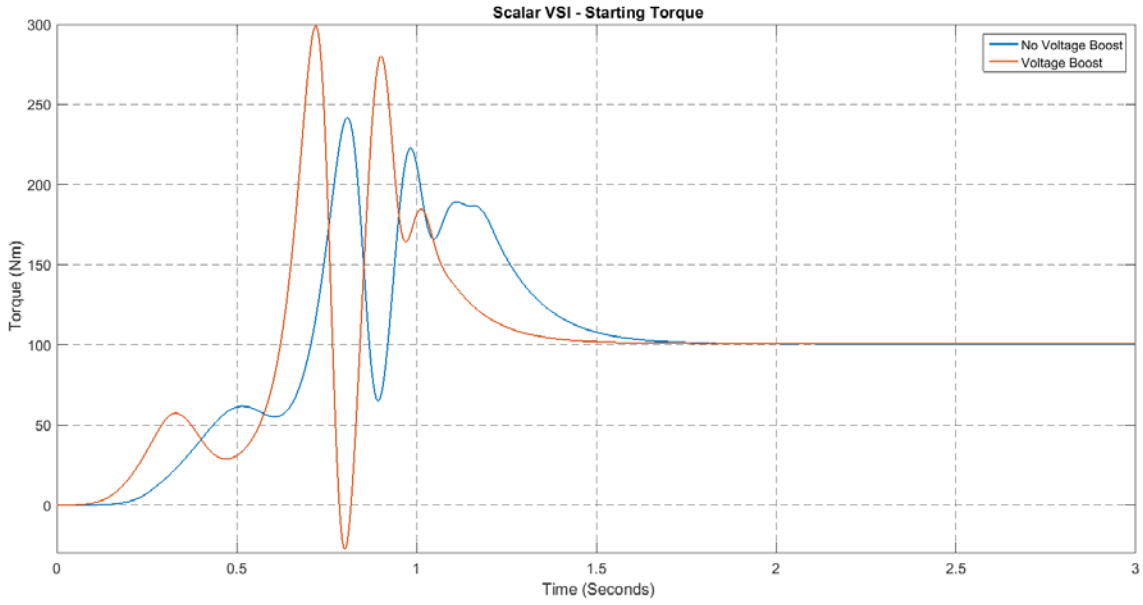

Figure 28: Starting Torque - Scalar VSI

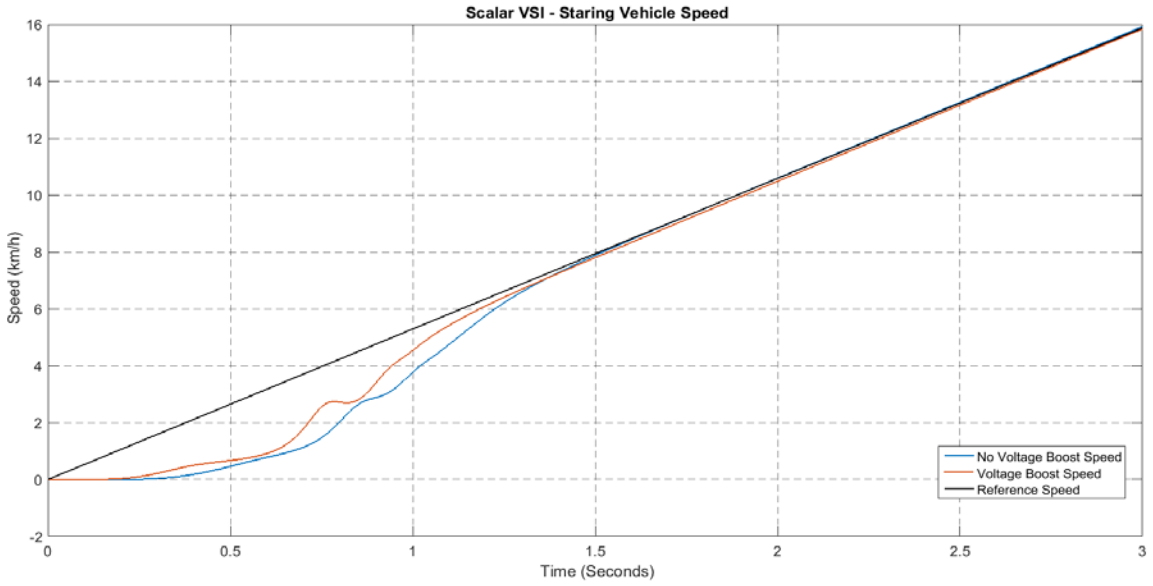

Figure 29 : Speed Profile with VSI Scalar

The simulation was run for 3 seconds with and without a voltage boost. For both techniques, the torque is slow to develop and there is significant torque oscillation. The torque oscillation is due to the transient offset in the stator currents. The offset in current produces an undesirable component of flux in the air gap which causes the torque oscillates. The observation from the voltage boosted system shows that the additional voltage increases the DC offset, which increases size of the oscillations. However, the increased voltage improves the torque response and decreases the period of the transients. While the poor starting performance was mentioned in the literature review, it was not shown how it would affect a vehicle. The simulation above shows that the performance is degraded for almost one second. The high frequency torque ripple is mostly filtered out by the large inertia of the vehicle; the slow response could be significant for vehicle application. Further simulations revealed that this degradation would last longer if a lower starting torque is applied versus a large one. This is due to the transient time constants dependence on the amplitude of the voltage applied. The transient dependence on the demanded torque is shown in the following graph.

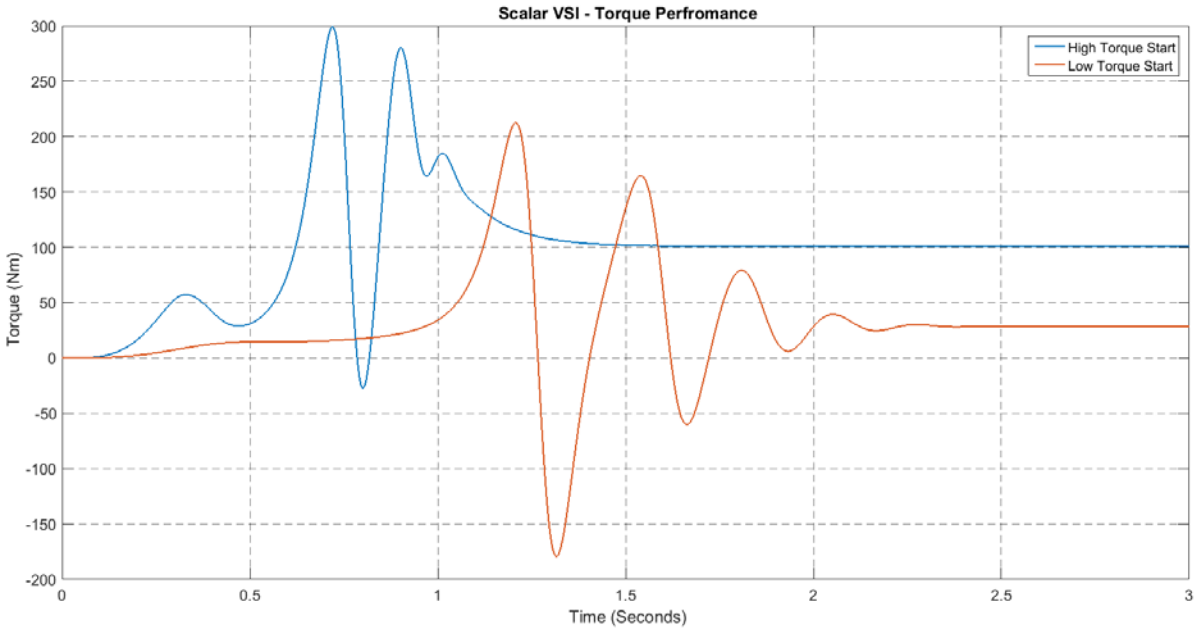

Figure 30 : Starting Transient Comparison

The graph above shows that a small torque demanded at start, the transients and torque response is prolonged. The smaller voltage applied to the windings increases the time constants for the inductive circuit. The torque does not settle on the demanded torque until ~2 seconds. This degradation to performance is too severe for typical commuter vehicles.

Two possible solutions to this starting transient were investigated in the remainder of the study. The first is to inject a high voltage at the start of the motor. The high voltage reduces the time constants of the inductive circuit in order to get better torque response. One way to produce this high voltage at start is to use a constant high slip frequency at start regardless of the torque demanded. Once the transient period is over, the controller switches to constant V/f control outline in section 3.5.1. This resolution stems from the

observations shown in Figure 27 with the addition of a voltage boost. Another way to improve starting performance is utilizing a current controlled voltage source inverter (CC-VSI) to ensure there is no DC offset component of current. The performance of these possible solutions will be investigated in the following sections.

7.1.1.1. Scalar - High Slip

One way to improve the starting torque performance is to minimize the time constants of the transients. As was discovered in the last section, these time constants depend on the voltage amplitude. A possible solution to this transient issue is reducing the transient time constants with a high starting voltage.

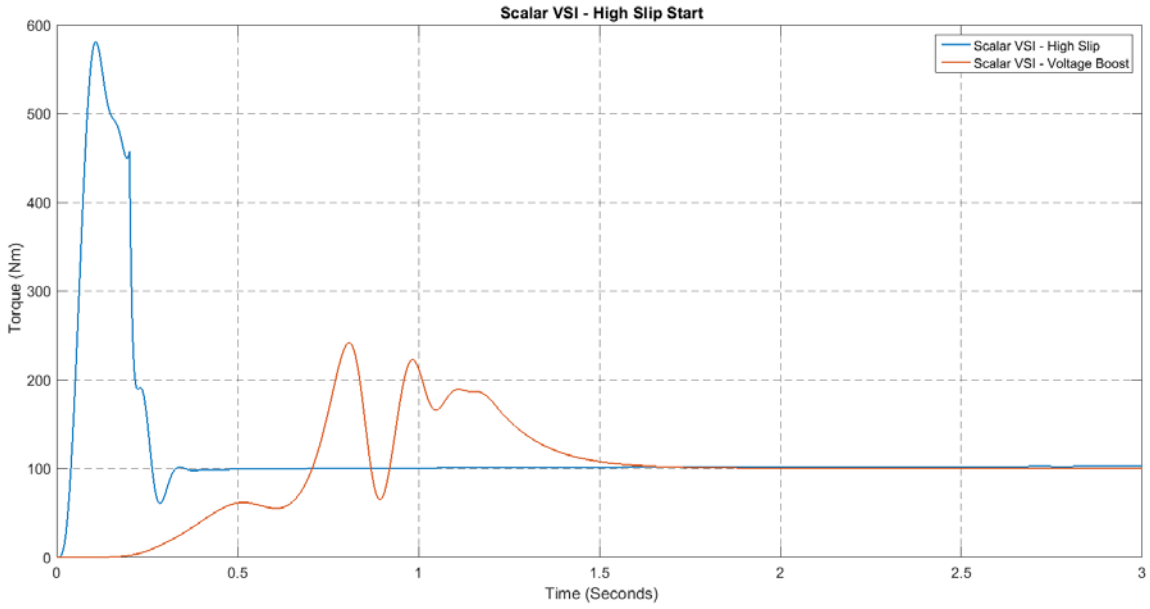

Figure 31 : Starting Performance with High Slip

In terms of constant V/f control, a large slip at start produces the desired high voltage. A simulation was run with a new scalar controller that starts with a constant high slip until the transients decay, then the controller switches to constant V/f operation. The results are shown given in Figure 31.

In the blue, the torque of the high slip scalar controller has a quicker response time. Regardless of the driver's input, the controller starts with this high slip resulting in a torque spike. The developed torque is much higher than desired. However, the torque spike has a very short sequence (<200ms). The transient time is decreases by greater than a factor of three from the standard constant V/f method with a voltage boost. The short pulse of torque is filtered greatly by the inertia of the vehicle. A discussion of the implications of this torque spike are given in the following paragraph considering some of the limitations of the model used during this simulation.

There are limitations of the induction and vehicle model that exacerbates the effect of the torque spike shown above. As detailed in the simulation section, the model does not consider saturation of iron because most of the operation of the motor is conducted within the reign of non-saturation. However, this starting condition operates well above the normal conditions. The iron would no longer be operating in the linear region and would saturate. This would reduce the developed torque and subsequent torque spike. During this short torque spike, the vehicle accelerates from 0-3 MPH. However, the vehicle model does not accurately reflect a real vehicles response in this instance. The model used for this vehicle is rigid without any dampening terms. A vehicle would not respond to a torque impulse of 200ms because of the elastic nature of the gears, shaft,

and tires. Additionally, there could be a clutch or an additional dampening device installed in the drive shaft which would soften this torque spike. Further testing, preferable with a physical motor and vehicle, would have to be done to determine how this start would be perceived by the driver and the long-term effects on the drivetrain of the vehicle.

The high slip method shortens the transients and improves the starting performance of the controller, even so, it is difficult to determine the overall effects of the starting method. There may be electrical and structural ramifications. This would require a more accurate model of the motor and vehicle to understand completely. A solution which does not create this large torque spikes is preferable.

7.1.1.2. Scalar - CC-VSI

The cause of the transient was identified as the transient offset in the stator current. This produces an unwanted flux that causes the torque oscillation. Additionally, the delay in current through the system due to the induction of the stator windings hinders the development of the flux in the airgap. A solution to this problem is utilizing a CC-VSI as mentioned in pervious sections 3.5.2. This method uses current sensors and hysteresis control to achieve motor control. Utilizing this method yields the following results during start.

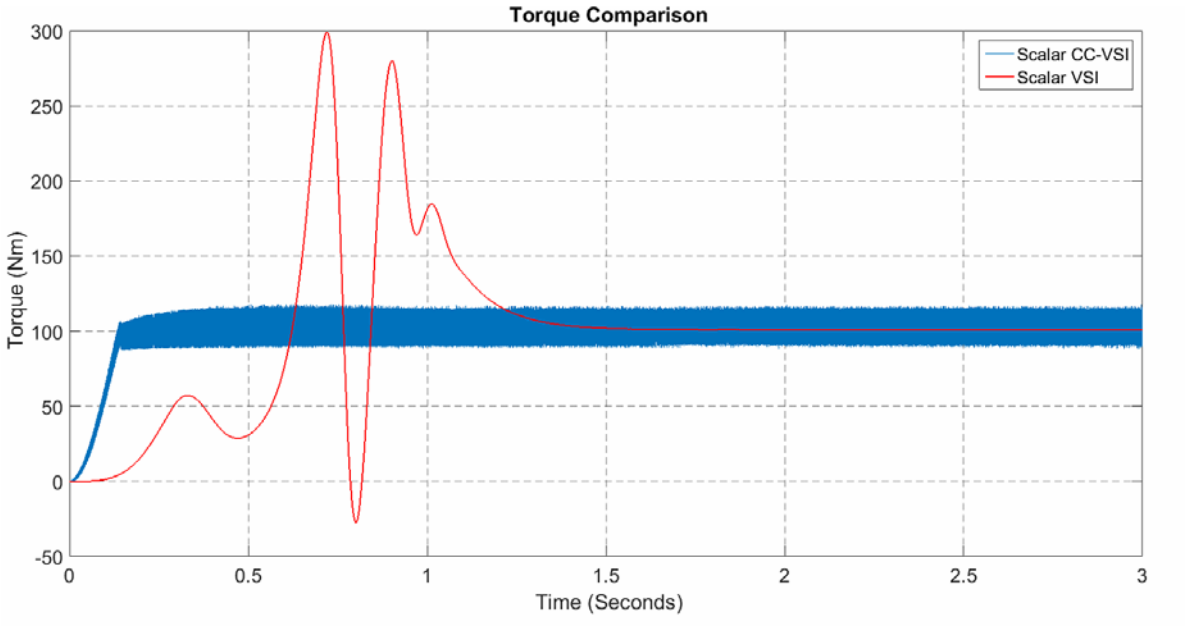

Figure 32 : Starting Performance

In the graph above, the CC-VSI controller is shown in blue. The developed torque no longer has a torque ripple and, furthermore, has a shorted response time. Note the noise in the torque signal from the scalar CC-VSI controller. In order to make this current controller, an ideal power electronic switching was emulated to implement the hysteresis control method outlined in section 3.5.2. The discontinuous square-wave voltage signals fed to the differential equations in the Simulink produces noise in the torque signal. This is an artifact of the simulation model. Nonetheless, the average value of torque is clear in the figure.

Additional information can be gleaned from observing the starting current for this method. The stator current during the start of the simulation is given below:

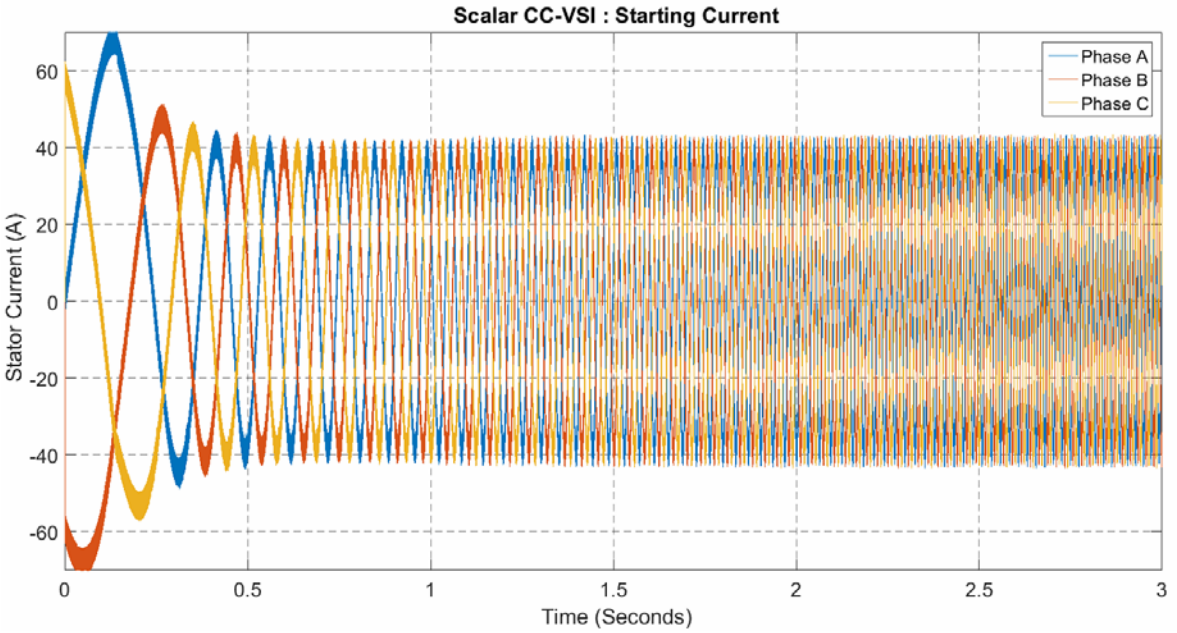

Figure 33 : Starting Current for Scalar CC-VSI

In order to minimize the torque response at the start, a higher current is applied at the beginning of the sequence. This higher-than-rated current reduces the time to generate flux in the airgap improving the torque response. In addition to the controls ability to shorten the torque response time by demanding a larger starting current, Figure 33 confirms that there is no current DC offset. This prevents any torque oscillation associated with the sudden application of voltage to the stator windings.

In general, the starting performance of this method is good. The torque delay leads to a small discrepancy in the speed of the vehicle. The difference in speed is 1 mph after 0.5 sec. This result was predicted in the introduction of this paper. It normal circumstances, the driver will demand more torque to compensate for the slower developed torque. Furthermore, the reactive nature of the PI controller used in this

simulation does not accurately model a driver, as stated in the limitations in section 6. In an actually vehicle, the driver would have demanded the torque prior to the vehicle acceleration. This time delay would be 100's of milliseconds, which is similar to many of the vehicles on the road today. Since drivers are accustom to this type of engine response, the difference delay torque response is inconsequential for this application.

This method had the best overall starting performance of the various scalar control methods. For the remainder of the study, this CC-VSI scalar method will be considered the preferable scalar method to pursue and compare with the vector control.

7.1.2. Vector Control - FOC

The following data was gathered from simulations using field oriented control (FOC). The first few seconds during the start were analyzed to compare with the pervious results for the scalar control methods. The results are shown below:

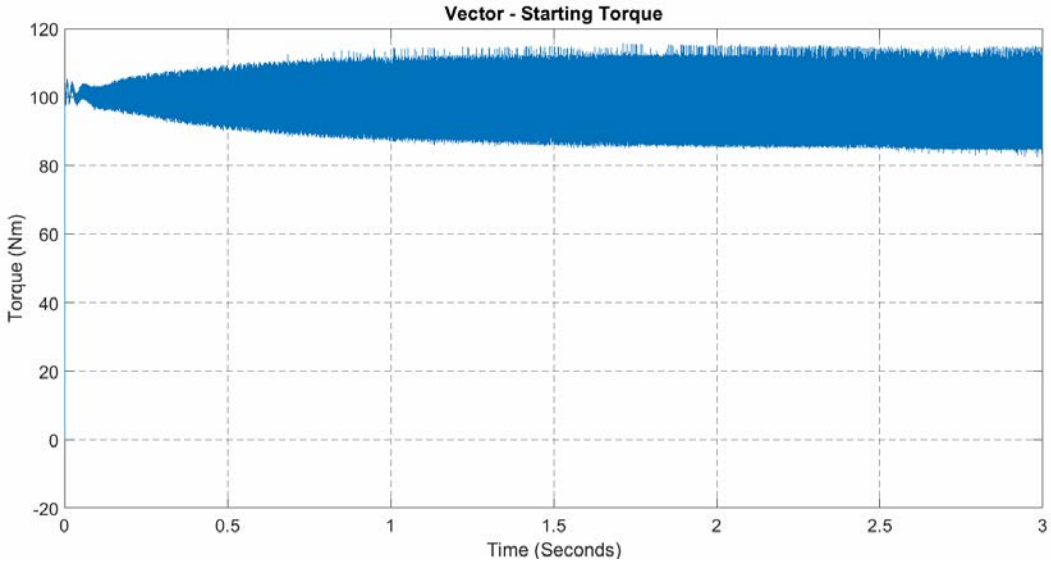

Figure 34 : Starting Torque for Vector Control

The torque control and response of the vector control is immediate during this simulation, taking only 10 milliseconds. Again, the torque contains a high frequency noise due to the simulated switching of ideal power electronics for a CC-VSI which is a requirement for FOC as outlined in section 3.5.3. The ability to quickly develop torque can be understood better from a review of the stator current.

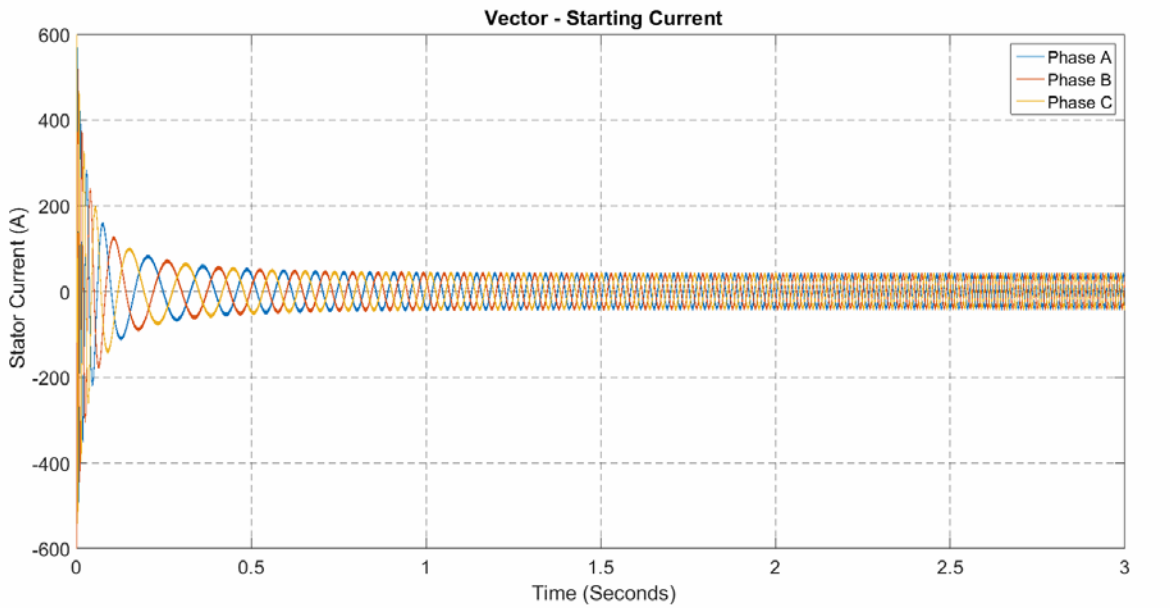

Figure 35 : Starting Current for Vector Control

The controller demands a large starting current to overcome the time constants of the stator windings to generate the flux in the airgap. Like the scalar CC-VSI method, this is an effective tool to improving the developed torque response. However, this controller does not have a limit on the current and, therefore, gives a current demand of x10 the rated current. Usually, it is acceptable to drive a motor with a larger-than-rated current for a short time before over heating becomes an issue. The duration and amplitude of

starting current is limited by the design and thermal management of the system. In order to compare the controls accurately, the same current limitations will be applied to the vector control as was done for the scalar CC-VSI controller.

The simulation was re-run with a current limitation similar to the CC-VSI scalar controller in the previous section. The data further supports the relationship between the starting current and torque response. The difference in performance does not depend on the type of motor control, but instead, on the limitation of the starting current. The torque and current from this simulation is shown below.

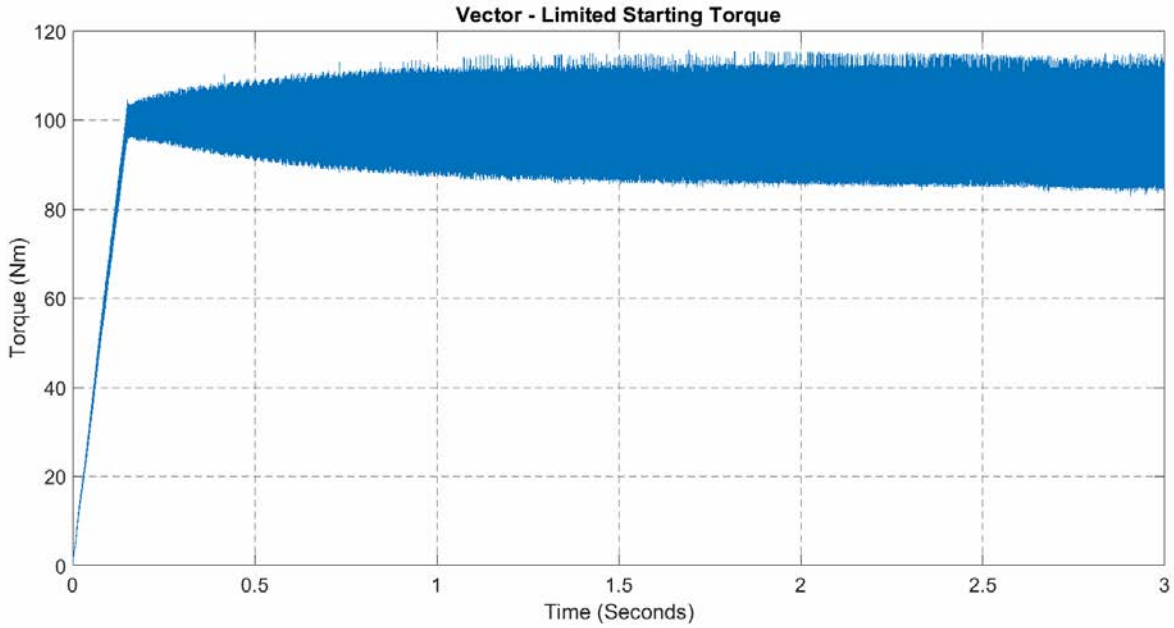

Figure 36 : Starting Torque for Vector Control with Current Limiter

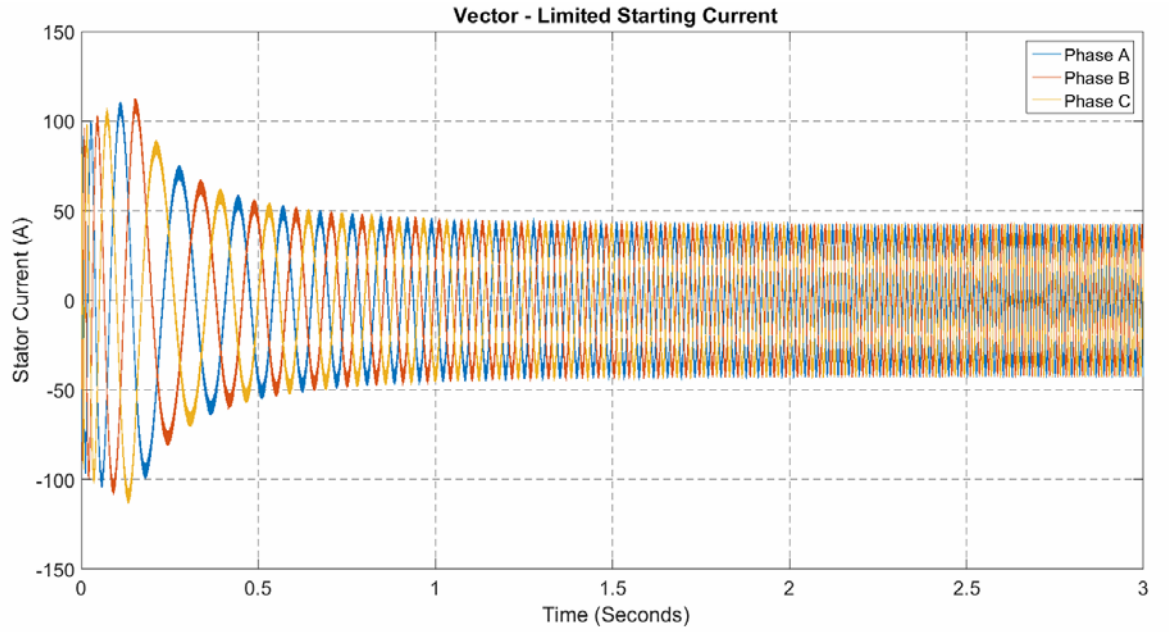

Figure 37 : Starting Current for Vector Control with Current Limiter

With the current limited, the torque takes 200 ms to develop, which is closer to the torque response of the scalar CC-VSI controller. The delayed torque response for such a large inertia vehicle plays a small role in the overall performance of the vehicle. Small speed discrepancies are either compensated by the driver or unnoticed. These preliminary results show trivial differences between the starting developed torque of the scalar CC-VSI control and the vector FOC control. Especially when limiting the starting current for the controllers.

Understanding the causes of these transients and applying sensical limitations has minimized the starting performance differences between the scalar and vector controllers. It is the intension to compare scalar control to the extremes of the performance capable of vector control. So, in the next simulations, the current

limitations will not be implemented on the vector control. This ensures that the simulation will test if nearly instant torque response is meaningful to vehicle performance.

7.2. FTP Drive Cycle

As verification that these controls could meet the dynamic requirements of a passenger vehicle, the entire FTP urban drive cycle was simulated for all three controls: constant V/f scalar control with high slip, scalar control that utilizes CC-VSI, and FOC without current limitation. The drive cycle last for 21 minutes and then repeats. First, the entire drive cycle will be shown for each control. The overview shows the torque and speed profiles for many scenarios. Since the cycle is long, some of the details can be lost in these graphs. So, in addition, individual moments of the cycle will be explored. The first graph shows the torque generated by the motors. The second shows the vehicle speed (in red) with the reference speed (in blue).

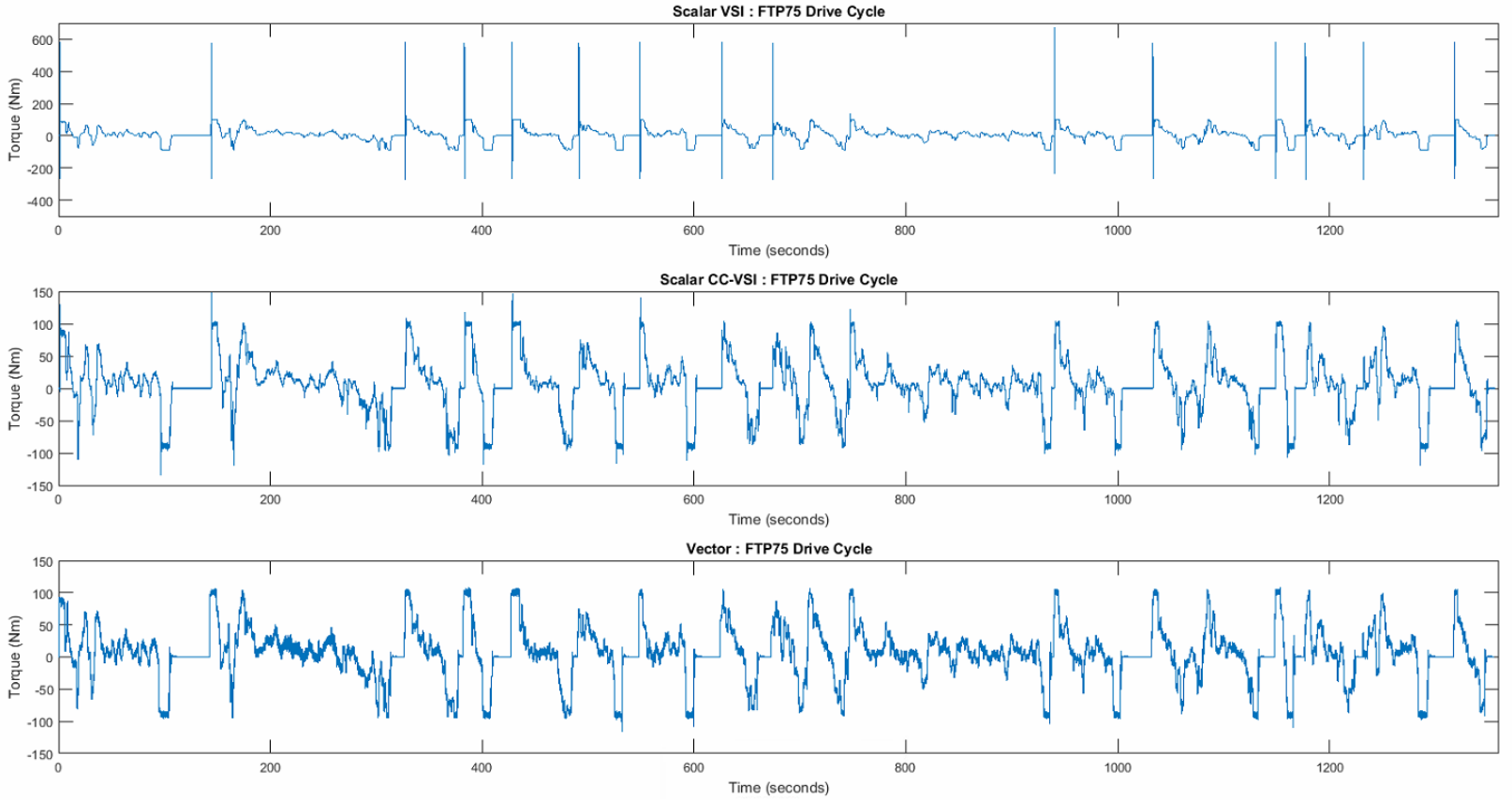

Figure 38 : FTP75 Drive Cycle - Developed Torque

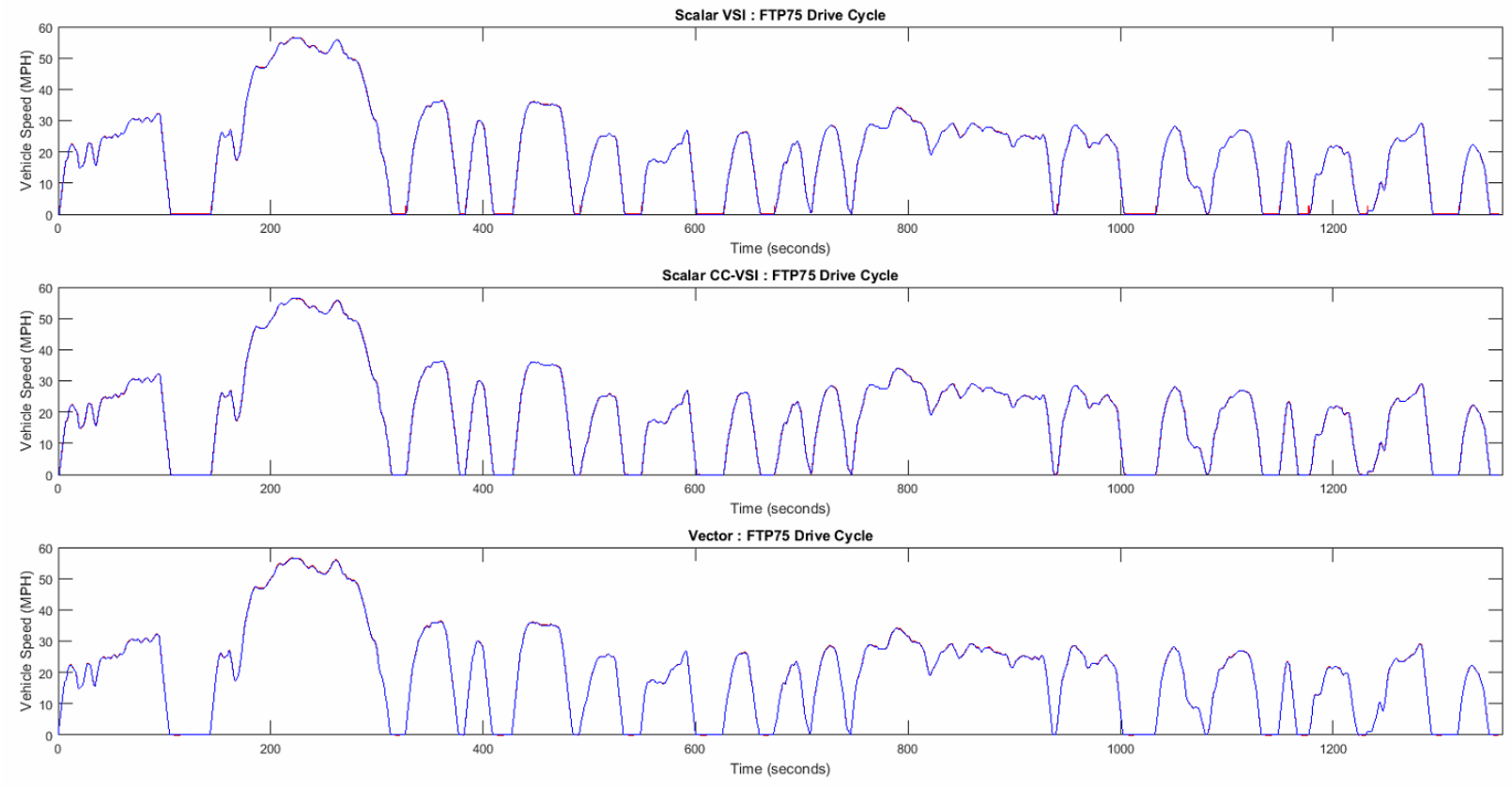

Figure 39 : FTP75 Drive Cycle - Speed Profile

Figure 38 shows the developed torque for each motor during the drive cycle. The VSI scalar control has large spikes of torque associated with the high slip frequency start. These short torque spikes lead to a discrepancy at the start of motor, but following the start, the motor tracks the FTP speed profile accurately. As mentioned previously, the effects of the large starting torque are overstated for several reasons. Even with the exaggerated effects of the torque spike, the motor is able to perform.

The data from the CC-VSI scalar and vector simulations reveals that the develop torques are similar. Since there was a short delay in developed torque with the CC-VSI scalar, the PI controller compensated with an overshoot to drive the speed error to zero. Excluding the start, the torque profiles are similar. Reviewing the speed profiles, there is no significant errors in speed in either simulations.

In order to observe the differences between the controls, it is helpful to look at smaller timescales of the FTP-75 cycle. Since the CC-VSI scalar is a more viable control method than the large slip VSI controller, the rest of the result section will focus on the comparison of the CC-VSI scalar method with vector FOC controller.

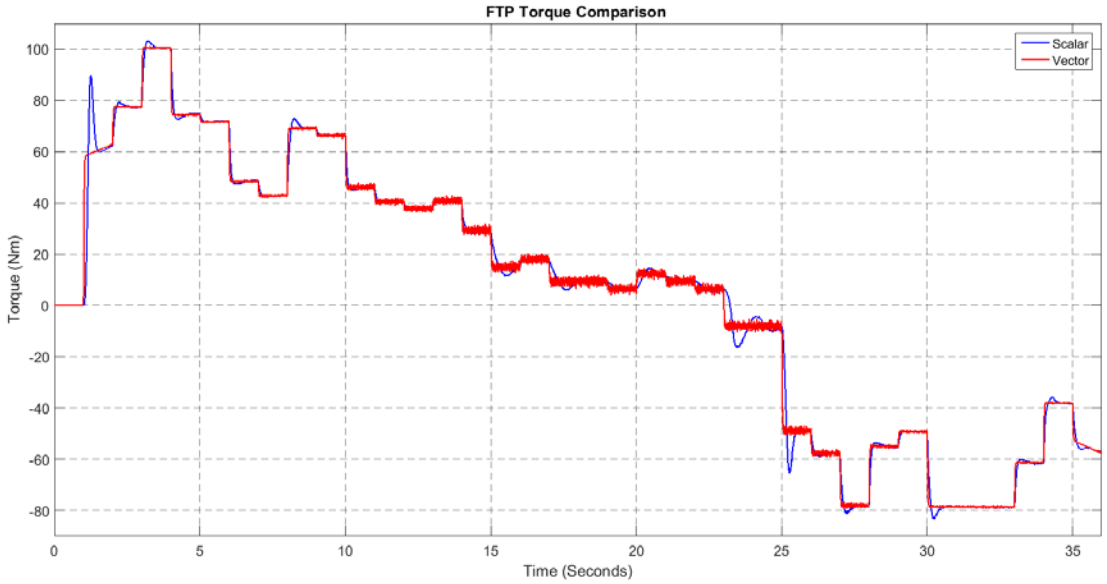

Figure 40 : FTP75 - Torque Comparison

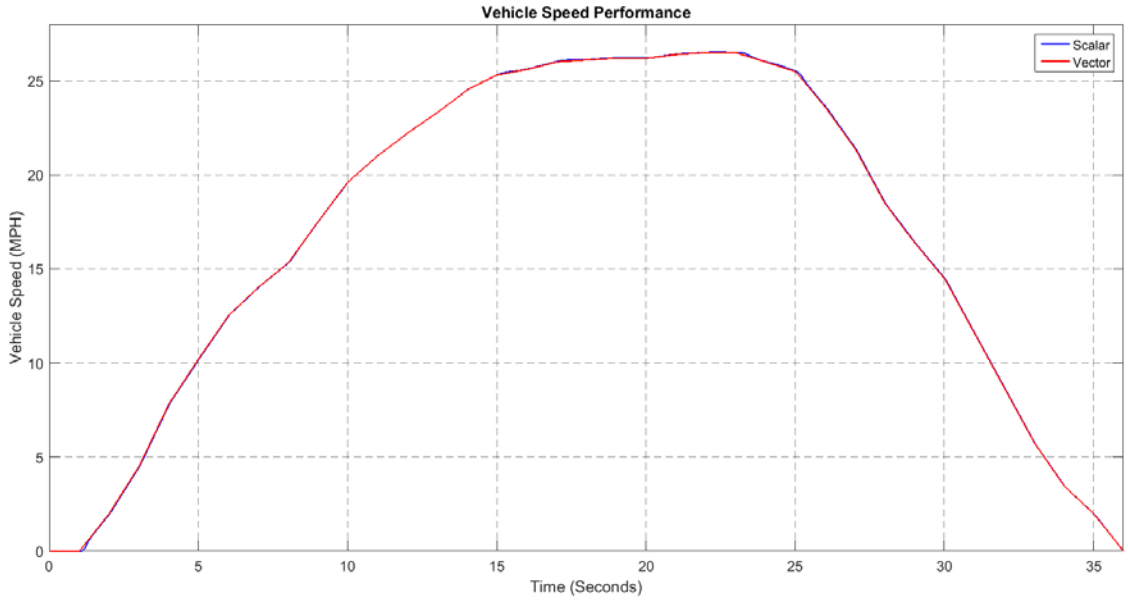

Figure 41 : FTP75 - Speed Comparison

The graphs show an entire ‘sequence’ of the FTP drive cycle from start to stop. The shorter time scale shows the difference in developed torque and speeds of the vehicle in more detail. The first observation to note is the starting performance. As the previous section showed, the vector control responds quickly from stand still. However, this simulation did not limit the starting current of the controller. This shows the best-case scenario for vector control. In contrast, the scalar control has a short, 250 ms delay. This leads to an overshoot by the PI controller to minimize the speed error. Moreover, the closed-loop and PI controller are reactive to the FTP speed curve. In reality, the driver of this car depressed the pedal several milliseconds before the speed of the vehicle started to accelerate (especially if the vehicle powered by an ICE). All of these factors indicate that the difference at start does not affect the driver’s experience or the vehicles performance.

After the start, another non-natural effect is shown in the simulation. Since the FTP-75 drive cycle records vehicle speed every second, this means that the change in speed needs to be interpolated between those data points. It follows that the slope changes at a minimum every second, and therefore, the acceleration of the vehicle changes instantly at this moment. This sudden change in acceleration requires an instantaneous change in torque demand. These discrete changes can be seen in the torque graph as torque steps in Figure 40. As stated in the introduction of this paper, in actuality, torque steps do not occur. Instead the driver steadily increases the acceleration with the pedal over 10s to 100s of milliseconds. The discretized changes in torque exaggerate the difference between the two control methods. The torque demand changes suddenly, and the

motor's developed torque needs to change to the value. The vector control method is able to do this quickly, while the scalar cannot. This phenomenon is better illustrated in the following graph, which is a smaller time frame of the same FTP 'sequence'.

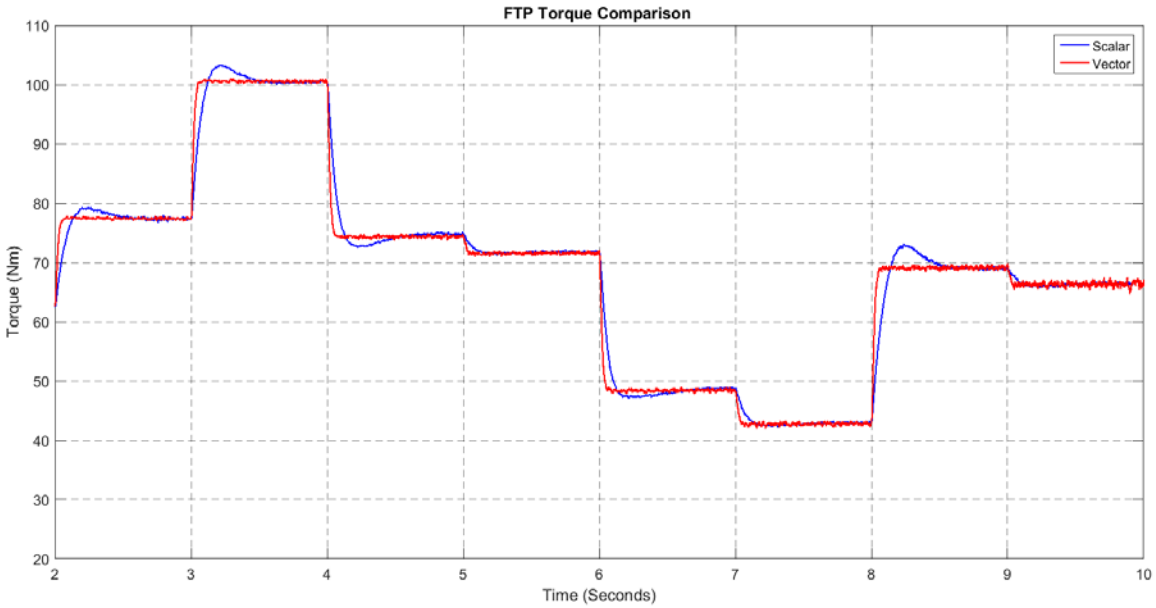

Figure 42 : Torque Comparison - Short Time Scale

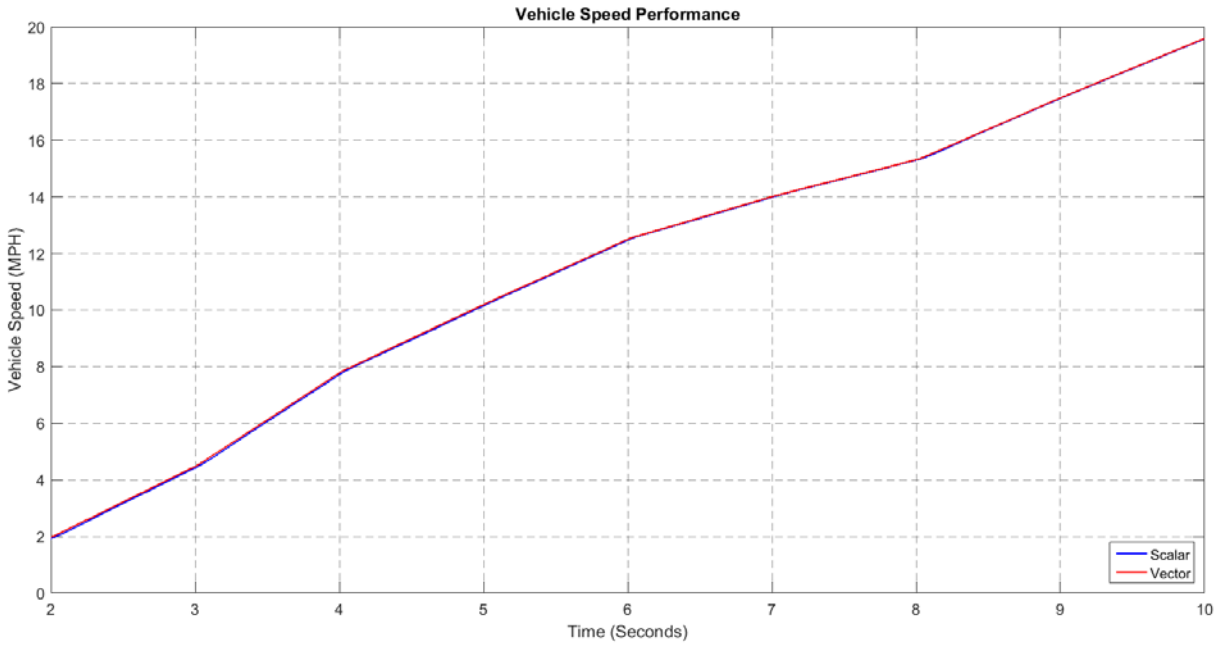

Figure 43 : Speed Comparison - Short Time Scale

The figures above show the discrete changes in torque demand that happen every second. The vector control motor is able to produce the various torque demands rapidly in 10's of milliseconds. Conversely, the scalar control takes approximately a 100 millisecond. Regardless of the torque response, the speed of the vehicle stays close to the FTP reference speed. Within a few tenths of the reference speed in MPH. Since the speed of the vehicle is the desired quantity for a vehicle, meeting this speed profile proves that the wanted performance is met. Even with the limitations of discrete data in the simulation/model, the performance of the controllers do not show an obvious preference towards vector control.

This section discussed the results of the simulation of the various control methods used to drive the modelled EV. The main observations such as starting torque, speed, and current were illustrated and explained. Then the entirety of the FTP drive cycle was analyzed. In order to distinguish more detail between the controls, specific moments of the cycle were presented. In light of the equivalences in performance of the two vehicles that utilize these different controls, the results are in line with the thesis statement of this research. The conclusions of this paper will be given in the next section.

8. CONCLUSION

This section discusses the conclusions drawn from the given results shown in the previous section. A brief summary of the novel ideas presented in this paper are reiterated. Then the implications of the results are offered in the conclusion. The scope of future research and recommendations are addressed at the end of this section.

8.1. Summary

This thesis purposes scalar based IM control methods as a viable option for traction applications. This opposes the common held belief that a dynamic, high performance application, such as vehicles, require costly and complex vector control methods. In order to determine the ramifications of this novelty, a more holistic simulation method was utilized. The trend in the current literature in this field is to test motor control methods without considering many of the following topics, which can have significant effects on comparison of the performance between the controls.

The design of the motor was carried out to ensure the properties of a typical traction motor for EV applications was accounted for. This entailed the appropriate sizing of the motor in both power and speed. Another unique consideration taken into account was the common practice of using high speed motors and utilizing a single ratio gearbox to reach the appropriate speeds for the vehicle tires. This technique shrinks the physical size of the motor which is critical for traction applications. The ramifications of this design are high frequency operation, lower currents, and higher voltages. These characteristics can have effects on the transients and overall performance of the motor

when implementing different controls methods. So, it is important to consider these topics when modeling an electric vehicle to determine the performance of various control methods.

Careful attention was paid to the load on the motor. The type of load plays a large role in the response of the motor. Since the application of electric motors to vehicle is not an established field, it was important to consider all the implications of this new load. The load that a vehicle presents to a motor is highly inertial with unpredictable resistive forces stemming from road conditions and air resistance. The load dictates how the driver will perceive the performance of the traction motor.

The final topic of interest were the speed profile of common passenger vehicles. The speed profile is the desired result from the driver's perspective. This is how the performance of the traction motor should be measured. The speed profile of a vehicle is highly dynamic with many unpredictable torque demands that require 'quick' response. However, because of the highly inertial nature of a vehicle, these changes in speed have large timescales when compared to motor response times.

These topics are the insights given in the paper to accurately compare the performance of scalar and vector control methods.

8.2. Conclusion

With these topics considered, the simulation of an electric vehicle utilizing the different control strategies was carried out. The results showed a small variance in the speed profiles of the two methods. The largest differences were seen during the starting transients of the motor. The differences were mitigated by implementing a CC-VSI for

the scalar control. The other notable variances were seen in the slower torque response times of the scalar method. However, since the torque response time have such small-time scales, the large inertia vehicle showed little difference in speed profiles which would lead to an indiscernible performance difference from the driver's perspective. Additionally, the discrete nature of the FTP data in combination with the reactive properties of the PI controller closed-loop speed control only exaggerate the difference in performance between the controls. These are artifacts of the simulation and do not reflect a true driver/vehicle system. This work is primarily an engineer design study to lead the way to implementing simpler controls for vehicle. The true impact of the different controls cannot be realized until they are implemented on a vehicle. However, the results of this paper justify the pursuit of a test on a physical vehicle to capture all the subtle and complexities of a passenger vehicle.

8.3. Future Work

With the results supporting the thesis of this paper, the following section discusses the suggested areas of further investigation on this topic.

In section 2, the subject of efficiency optimization was evaluated as an important parameter for a control method in electric vehicles. Yet, the ability to optimize was not dependent on the type of control (scalar or vector), so the subject was not a focus for this paper. Still, the type of efficiency optimization would affect the performance of the vehicle. Efficiency optimization in electric motors tend to use field weakening techniques to reduce the losses in the motor when operating in certain conditions. This field weakening can reduce the torque response for the motor regardless of control

method. This approach should include all aspects of the vehicle powertrain and mechanics, including the battery, inverter, motor, and vehicle. An in-depth look at the appropriate efficiency optimization method for scalar method would provide further knowledge of the system and its performance.

Throughout this research, there were only three control algorithms used in the simulation. For scalar, the two methods were constant V/f and a CC-VSI control method based on the scalar model. For vector, the only method investigated was FOC. These methods were chosen, in part, due to their popularity, but many more methods within the scalar and vector categories should be considered. Including novel scalar controls for the specific use in vehicle applications.

The new technological advancements in autonomous vehicles also presents a unique opportunity for research in motor control techniques. Many of the unpredictable behavior of vehicle applications stems from the driver. With autonomy, there will be predictive demands for the motor possibly for the entire ride prior to leaving the driveway. This pivotal change to traction applications will require further research in motor control methods.

REFERENCES

[1] J. Romm, "The car and fuel of the future," *Energy Policy,* vol. 34, no. 17, pp. 2609-2614, 2006/11/01/ 2006.

[2] V. C. Mikhail and H. Arpad, "Environmental assessment of passenger transportation should include infrastructure and supply chains," *Environmental Research Letters,* vol. 4, no. 2, p. 024008, 2009.

[3] P. D. Department of Economics and Social Affairs, United Nations, , "World Population Prospects: The 2015 Revision, Key Findings and Advance Tables," vol. Working Papar No. ESA/P/WP.241, 2015.

[4] J. Pucher, N. Korattyswaropam, N. Mittal, and N. Ittyerah, "Urban transport crisis in India," *Transport Policy,* vol. 12, no. 3, pp. 185-198, 2005/05/01/ 2005.

[5] W. Sung, J. Shin, and Y. s. Jeong, "Energy-Efficient and Robust Control for High-Performance Induction Motor Drive With an Application in Electric Vehicles," *IEEE Transactions on Vehicular Technology,* vol. 61, no. 8, pp. 3394-3405, 2012.

[6] N. Sharma and V. K. Garg, *A Comparative Analysis of Scalar and Vector Control of Induction Motor Drive* (Impending Power Demand and Innovative Energy Paths).

[7] L. K. Jisha and A. A. P. Thomas, "A comparative study on scalar and vector control of Induction motor drives," in *2013 International conference on Circuits, Controls and Communications (CCUBE),* 2013, pp. 1-5.

[8] G. Kohlrusz and D. Fodor, "Comparison of Scalar and Vector Control Strategies of Induction Motors," *Hungarian Journal of Industrial Chemistry,* vol. 39, no. 2, pp. 265-270, 2011.

[9] H. Rehman, "Detuning minimization for alternative energy vehicular drive system," in *2012 IEEE Vehicle Power and Propulsion Conference,* 2012, pp. 42-47.

[10] A. Emil Hasan, H. Hassan, and I. Bugis, "Variable Speed Vector Control for Induction Motor of Electric Vehicle," *Applied Mechanics & Materials,* Article vol. 699, pp. 759-764, 11/13/ 2014.

[11] O. Ellabban, J. V. Mierlo, and P. Lataire, "A comparative study of different control techniques for an induction motor fed by a Z-source inverter for electric vehicles," in *2011 International Conference on Power Engineering, Energy and Electrical Drives*, 2011, pp. 1-7.

[12] K. T. Chau and Z. Wang, "Overview of power electronic drives for electric vehicles," *HAIT Journal of Science and Engineering*, vol. 2, no. 5-6, pp. 737-761, June 16 2005 2005.

[13] V. K. Gupta, B. Tiwari, and B. Dewangan, "Efficiency Optimization of Induction Motor Drive: A Review," *International Journal of Innocative Sciency, Engineering & Technology*, vol. 2, no. 12, pp. 650-655, 2015.

[14] P. Melo, R. d. Castro, and R. E. Araújo, "Evaluation of an Energy Loss-Minimization Algorithm for EVs Based on Induction Motor," in *Induction Motors - Modelling and Control*, P. R. E. Araújo, Ed. Rijeka: InTech, 2012, p. Ch. 17.

[15] J. G. Cleland, V. E. McCormick, and M. W. Turner, "Design of an efficiency optimization controller for inverter-fed AC induction motors," in *Industry Applications Conference, 1995. Thirtieth IAS Annual Meeting, IAS '95., Conference Record of the 1995 IEEE*, 1995, vol. 1, pp. 16-21 vol.1.

[16] M. Ehsani, Y. Gao, and A. Emadi, *Modern Electric, Hybrid Electric, and Fuel Cell Vehicles*, 2nd ed. Boca Raton: CRC Press, 2010.

[17] P. Krause, O. Wasynczuk, S. Sudhoff, and S. Pekarek, J. Anderson, Ed. *Analysis of Electric Machinery and Drive Systems*, 3rd ed. Piscataway, NJ: IEEE Press, 2013.

[18] Mathworks. (2017, January 14). *Simulate an AC Motor Drive*. Available: https://www.mathworks.com/help/physmod/sps/powersys/ug/simulating-an-ac-motor-drive.html

[19] A. Cifci, Y. Uyaroglu, and S. Birbas, *Direct Field Oriented Controller Applied to Observe Its Advantages over Scalar Control* (2012, no. 3). 2012.

[20] S. S. Emani, "Performance Evaluation of Cascaded H-Bridge Multi-level Inverter FED BLDC Motor Drive In an Electric Vehicle," Electrical Engineering Master of Science, Electrical & Computer Engineering, Texas A&M University, 2010.

[21] M. Farasat, A. M. Trzynadlowski, and M. S. Fadali, "Efficiency improved sensorless control scheme for electric vehicle induction motors," *IET Electrical Systems in Transportation*, vol. 4, no. 4, pp. 122-131, 2014.

[22] P. Procházka, B. Klíma, P. Vorel, and P. Huták, "Small electric vehicle drive control according to maximal efficiency criteria," in *2011 IEEE International Symposium on Industrial Electronics*, 2011, pp. 745-749.

[23] R. Marino, S. Scalzi, and C. M. Verrelli, "Speed and Traction Control in Electric Vehicles with Induction Motors," Electrical Engineering, Electronic Engineering Department, University of Rome Tor Vergata, Rome, Italy, 2012.

[24] L. Chen, X. Sun, H. Jiang, and X. Xu, "A High-Performance Control Method of Constant V/f-Controlled Induction Motor Drives for Electric Vehicles," *Mathematical Problems in Engineering*, Research vol. 2014, p. 10, 21 January 2014 2014.

[25] G. EI-Saady, E.-N. A. Ibrahim, and M. Elbesealy, "A Fuzzy V/F Control for High Performance Induction Motor Drives," *SOP Transactions on Power Transmission and Smart Grid*, 2015.

[26] A. Munoz-Garcia, T. A. Lipo, and D. W. Novotny, "A New Induction Motor Open-Loop Speed Control Capable of Low Frequency Operation," Electrical Engineering, Department of Electrical and Computer Engineering, University of Wisconsin-Madison, Madison, WI, 579-586, 1997.

[27] J. Pongpant, S. Po-ngam, and M. Konghirum, "The Performance Improvement of Constant V/f Control of Induction Motor Drive in Low Speed Range," Electrical Engineering, Deparment of Electrical Engineering, King Mongkut's University of Technology Thonburi, Bangkok, Thailand.

[28] A. Smith, S. Gadoue, M. Armstrong, and J. Finch, "Improved method for the scalar control of induction motor drives," *IET Electric Power Applications*, vol. 7, no. 6, pp. 487-498Available: http://digital-library.theiet.org/content/journals/10.1049/iet-epa.2012.0384

[29] M. Wüst *et al.*, "Operating strategy for optimized CO2 and NOx emissions of diesel-engine mild-hybrid vehicles," in *15. Internationales Stuttgarter Symposium: Automobil- und Motorentechnik*, M. Bargende, H.-C. Reuss, and J. Wiedemann, Eds. Wiesbaden: Springer Fachmedien Wiesbaden, 2015, pp. 93-111.